DOI: 10.1002/ejic.201001363

Two-Step versus One-Step Spin Transitions in Iron(II) 1D Chain Compounds

Wolfgang Bauer,[a] Wolfgang Scherer,[b] Sandra Altmannshofer,[b,c] and Birgit Weber*[a,d]

Dedicated to Professor Peter Klüfers on the occasion of his 60th birthday

Keywords: Iron / N,O ligands / Magnetic properties / Spin crossover / X-ray structure analysis

Eleven iron(II) 1D coordination polymers with the general formula $[FeL_{eq}(L_{ax})]$·solvent were synthesised and characterised, where L_{eq} = (E,E)-{diethyl 2,2′-[1,2-phenylenebis(iminomethylidyne)]bis(3-oxobutanato) (2-)-*N*,*N*′,O^3,O$^{3′}$} (L1) and {[3,3′]-[1,2-phenylenebis(iminomethylidyne)]bis(2,4-pentane-dionato)(2-)-*N*,*N*′,O^2,O$^{2′}$} (L2); L_{ax} = 4,4′-bipyridine (bipy), 1,2-bis(4-pyridyl)ethane (bpea) and 1,3-bis(4-pyridyl)propane (bppa) and solvent = MeOH, EtOH and toluene (Tol). [FeL1(bpea)]·MeOH (**3**·MeOH) shows an abrupt one-step spin crossover with thermal hysteresis (27 K) and [FeL2(bppa)]·MeOH (**2**·MeOH), [FeL2(bpea)] (**4**), [FeL2(bpea)]·0.25MeOH (**4**·0.25MeOH) and [FeL1(bipy)]·MeOH (**5**·MeOH) show a two-step spin transition with an IP at $\gamma_{HS} \approx 0.5$ (IP is intermediate plateau and γ_{HS} is high-spin mol fraction) and up to 50 K wide hysteresis loops (**5**·MeOH). [FeL1(bppa)] (**1**), [FeL2(bppa)]·EtOH (**2**·EtOH) and [FeL1(bpea)]·1.5Tol (**3**·1.5Tol) show an abrupt incomplete spin transition that stops at $\gamma_{HS} \approx 0.5$; for [FeL1(bppa)]·0.25MeOH (**1**·0.25MeOH) and [FeL1(bpea)] (**3**), the spin transition is gradual and incomplete. The X-ray crystal structures of six complexes were determined (**1**, **2**·MeOH, **3**·MeOH, **3**·1.5Tol, **4**·0.25MeOH and **5**·MeOH). In the case of **4**·0.25MeOH, the crystal structures for the HS and LS states were dertermined; for compounds **1**, **2**·MeOH and **3**·1.5Tol, the crystal structure of the HS and the IP state was investigated. For all complexes, the iron(II) centre is located in a distorted octahedral coordination sphere. Each axially coordinated ligand "connects" two iron(II) centres, which results in the formation of extended 1D chains with varying structures from linear (bipy) over steplike (bpea) to zigzag (bppa). Analysis of the intermolecular interactions reveals that the hysteresis width depends on both the stiffness of the axial ligand and the number of intermolecular contacts, while zigzag chains support stepwise spin transitions.

Introduction

The bistability of spin-transition complexes (spin crossover, SCO) is one of the most promising characteristics for new electronic devices in molecular memories and switches as it may be controlled by different physical perturbations such as temperature, pressure or light.[1,2] Of the possible types of spin transition (gradual, abrupt, with hysteresis, stepwise, incomplete), much of the interest is focused on the bistability in highly cooperative systems (hysteresis or memory effect) as such compounds can exist in two different electronic states depending on the history of the system. Various examples in the literature[1,3] as well as in our group[4] demonstrate that the control over intermolecular interactions is a central point for the control of cooperative interactions. With regard to this, we recently characterised an iron(II) spin-crossover complex with a 70 K wide thermal hysteresis loop at around room temperature based on a 2D network of hydrogen bonds between the complex molecules.[5] Next to highly cooperative systems, stepwise transitions between three or more states have attracted the interest of several research groups, because of the versatile switching possibilities.[6] This type of SCO is most frequently obtained for binuclear complexes and explained with the formation of [HS–HS], [HS–LS] and [LS–LS] spin-pair states (where HS and LS represent the local high-spin and low-spin states of the binuclear species with $S = 2$ and $S = 0$ for d^6), which could be directly monitored, for example, by Mössbauer spectroscopy and switched selectively by different wavelengths.[6] Results from DFT calculations agree with the conclusion of the phenomenological model, that the enthalpy of the [HS–LS] state must be lower than the average enthalpy of the [LS–LS] and the [HS–HS] states to create conditions for a two-step transition (assuming that in the [HS–HS] and [LS–LS] states both iron centres are

[a] Center for Integrated Protein Science Munich at the Department Chemie und Biochemie, Ludwig-Maximilians- Universität München,
Butenandtstr. 5-13 (Haus F), 81377 München, Germany
[b] Universität Augsburg, Institut für Physik, Lehrstuhl für Chemische Physik und Materialwissenschaften,
86135 Augsburg, Germany
[c] Georg-August-Universität Göttingen, Institut für Anorganische Chemie,
Tammannstraße 4, 37077 Göttingen, Germany
[d] Inorganic Chemistry II, Universität Bayreuth,
Universitätsstraße 30, NW I, 95440 Bayreuth, Germany
Fax: +49-92155-2157
E-mail: weber@uni-bayreuth.de
Supporting information for this article is available on the WWW under http://dx.doi.org/10.1002/ejic.201001363.

equivalent).[7] Another possibility for having a multistep spin transition is attributed to two (or more) different spin-crossover sites, each undergoing a transition at different temperatures.[8] Finally, there are examples of mononuclear complexes with a unique crystallographic iron(II) site where two nonequivalent iron(II) sites appear upon cooling as a result of a crystallographic phase transition. In these cases, the effects of ferromagnetic-type long-range and antiferromagnetic-type short-range interactions of an elastic origin are responsible for steps in the transition curve.[9,10] The most frequently used tool to assign SCO compounds with stepwise spin transitions to one of the three possibilities is X-ray structure analysis. The most obvious case (and also the most common one) is to have multiple crystallographic distinct metal centres at all temperatures. The often very subtle differences between the SCO sites are most likely the reason for the observed stepwise spin transitions. This also accounts for binuclear complexes. The compound $[Fe(NCS)_2(ddpp)]_2{\cdot}4(CH_2Cl_2)$ [with ddpp = 2,5-(di-2-pyridylamine)pyridine] was the first example of a binuclear complex where an ordered [HS–LS] state was observed at the intermediate-plateau (IP) temperature. However, this compound has two nonequivalent iron sites at all temperatures, which is most likely the reason for the stepwise spin transition.[11] Recently, the first examples of a 1D polymeric material undergoing a two-step spin transition were presented by Neville, Murray and co-workers.[12] Of the two compounds presented that have a stepwise spin transition, results from X-ray analysis reveal that one ($[Fe(NCS)_2(bdpp)]$, with bdpp = 4,6-bis(2′,2′′-pyridyl)pyrazine), has two distinct iron(II) centres at each temperature with ordered, alternating HS and LS sites at the intermediate-plateau temperatures. In contrast to this, the second compound ($[Fe(NCSe)_2(bdpp)]$) has one unique iron(II) centre at each temperature with an averaged HS/LS character at the IP temperature. For both possibilities, a clear assignment to one of the types of stepwise spin transitions is difficult, and the reason for the step in the transition curve cannot be given without doubt.[12]

One of the major goals in spin-crossover research is to develop rules that allow the synthesis of spin-crossover materials with predictable properties. Detailed magnetic and structural analyses of spin-crossover systems in combination with a comparison between the different systems are necessary to reach this point. The system investigated by our group is highly suitable for performing systematic investigations on structure–property relationships. The octahedral coordination sphere around the iron(II) centre is generated by a Schiff base like N_2O_2 coordinating ligand that occupies the equatorial plane. With pyridine- or imidazole derivatives at the axial sites, SCO behaviour is observed quite frequently.[13] The replacement of the monodentate pyridine by bidentate ligands such as 4,4′-bipyridine (bipy), 1,2-bis(4-pyridyl)ethane (bpea) or 1,3-bis(4-pyridyl)propane (bppa) results in the formation of 1D coordination polymers with the general formula $[FeL_{eq}(L_{ax})]{\cdot}$solvent. A schematic representation of the ligands discussed in this work is given in Scheme 1. The combination of two equatorial and three axial ligands in different solvents leads to a series of 13 compounds, summarised in Table 1, of which the pair [FeL2(bipy)] (**6**)/[FeL2(bipy)]·0.25MeOH (**6**·0.25MeOH) is already published.[14] Detailed analyses of the structures and the magnetic properties of the remaining 11 compounds and comparisons with known 1D chain SCO materials allow the development of a first concept on how spin-crossover materials with stepwise spin transitions can be designed rationally and to confirm already existing ideas about cooperative interactions in chain compounds.

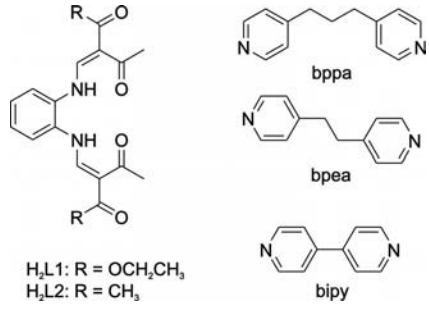

Scheme 1. Schematic representation of the ligands discussed in this work.

Results

Magnetic Susceptibility Studies of Thermally Induced SCO

The thermal dependence of the $\chi_M T$ product (χ_M is the molar susceptibility and T temperature) for all compounds measured is given in Figure 1. For purposes of completeness, the results of the magnetic measurements on compounds **6** and **6**·0.25MeOH[14] are given as well. Characteristic values of the susceptibility measurements are summarised in the Supporting Information, Table S1. The room

Table 1. Overview of the compounds discussed in this work with the used abbreviations.

Equatorial/ axial ligand	bppa	bpea	bipy
H_2L1	[FeL1(bppa)] (**1**)[a]	[FeL1(bpea)]·1.5Tol (**3**·1.5Tol)[a]	[FeL1(bipy)] (**5**)[b]
	[FeL1(bppa)]·0.25MeOH (**1**·0.25MeOH)[b]	[FeL1(bpea)] (**3**)[b]	[FeL1(bipy)]·MeOH (**5**·MeOH)[c]
		[FeL1(bpea)]·MeOH (**3**·MeOH)[c]	
H_2L2	[FeL2(bppa)]·EtOH (**2**·EtOH)[d]	[FeL2(bpea)] (**4**)[b]	[FeL2(bipy)] (**6**)[b][14]
	[FeL2(bppa)]·MeOH (**2**·MeOH)[b]	[FeL2(bpea)]·0.25MeOH (**4**·0.25MeOH)[c]	[FeL2(bipy)]·0.25MeOH (**6**·0.25MeOH)[c][14]

[a] Synthesised in or recrystallised from toluene. [b] Synthesised in methanol. [c] Crystals obtained by slow diffusion techniques in methanol. [d] Synthesised in ethanol.

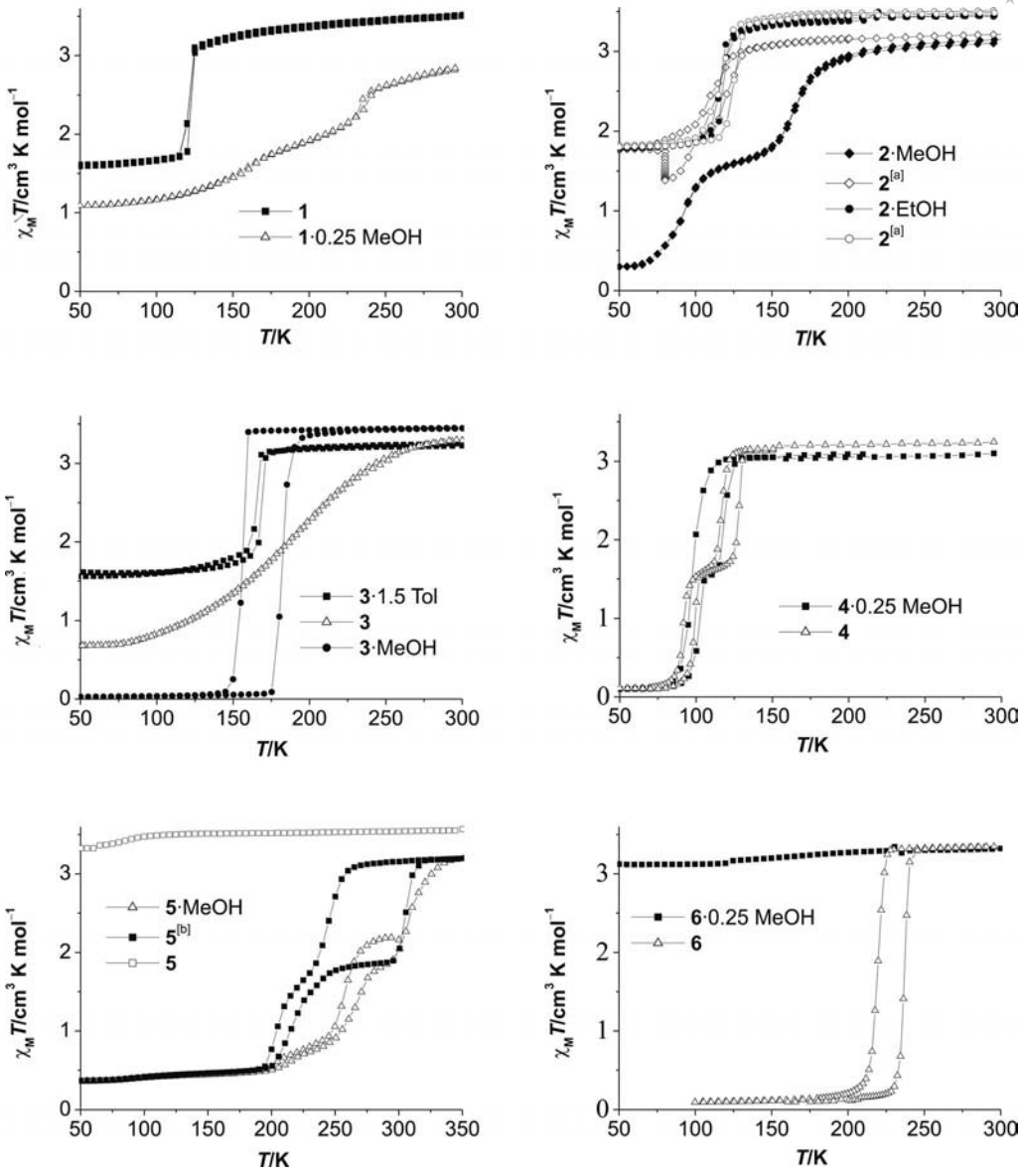

Figure 1. Plot of the $\chi_M T$ product vs. T for the different compounds discussed in this work. For completeness, the example of **6** and **6**·0.25MeOH[14] are given as well. [a] Tempered at 400 K for 1 h. [b] Heated to 350 K.

temperature $\chi_M T$ value of all compounds, with the exception of **5**·MeOH, are in the range of 3.25 $cm^3 K mol^{-1}$, typical for an iron(II) complex in the HS state. For **5**·MeOH, the room temperature moment is 2.19 $cm^3 K mol^{-1}$, which is significantly lower, but upon heating to 350 K, the moment increases to reach a value of 3.20 $cm^3 K mol^{-1}$. Upon cooling (starting from the pure HS state), various types of spin transition can be observed for the compounds. A complete, one-step spin transition is observed for the previously published compound **6**, which is accompanied by an 18 K wide thermal hysteresis loop ($T_C\downarrow$ = 219 K, $T_C\uparrow$ = 237 K)[14] and for **3**·MeOH, which is accompanied by a 27 K wide thermal hysteresis loop ($T_C\downarrow$ = 155 K, $T_C\uparrow$ = 182 K). For **1**·0.25MeOH and **3**, the spin transition is gradual and incomplete, with remaining $\chi_M T$ products at 50 K of 1.09 $cm^3 K mol^{-1}$ and 0.68 $cm^3 K mol^{-1}$, respectively. All the other examples show either a two-step spin transition with an IP at $\gamma_{HS} \approx 0.5$ (**2**·MeOH, **4**, **4**·0.25MeOH, **5**·MeOH) or an incomplete spin transition that stops at $\gamma_{HS} \approx 0.5$ (**1**, **2**, **2**·EtOH, **3**·1.5Tol). Compounds **5** and **6**·0.25MeOH[14] are HS in the entire temperature range investigated. The spin-transition behaviour of **5**·MeOH is more complex than those of the other examples: starting the magnetic measurement at room temperature, the $\chi_M T$ values decrease upon cooling, first gradually then more rapidly, then again gradually from 2.19 $cm^3 K mol^{-1}$ to attain a minimum value of 0.46 $cm^3 K mol^{-1}$ at 175 K. The $T_C\downarrow$ value is 255 K. Further cooling causes no significant decrease. The $\chi_M T$ value of 2.19 $cm^3 K mol^{-1}$ indicates that approximately two thirds of the iron(II) sites are in the HS state at room temperature. Upon heating, the $\chi_M T$ values increase between 200 and 280 K to attain a maximum value of 1.76 $cm^3 K mol^{-1}$,

which indicates that half of the iron(II) sites are in the HS state. The $T_C\uparrow(2)$ value of this step is 260 K. Above 280 K, the $\chi_M T$ values increase further to attain a maximum of 3.20 $cm^3 K mol^{-1}$ at 350 K, indicative of iron(II) in the HS state. The $T_C\uparrow(1)$ value of this step is 309 K. Between 245 and 300 K, the $\chi_M T$ values of the heating mode lie by an average of 0.50 $cm^3 K mol^{-1}$ lower than the values of the cooling mode. When starting the magnetic measurement at 350 K, the $\chi_M T$ values remain approximately constant upon cooling at 3.20 $cm^3 K mol^{-1}$ down to 270 K. Between 270 and 225 K, the $\chi_M T$ values rapidly decrease to a first minimum at 1.75 $cm^3 K mol^{-1}$. The $T_C\downarrow(1)$ value of this step is 245 K. Between 225 and 190 K, the $\chi_M T$ values further decrease to 0.50 $cm^3 K mol^{-1}$. The $T_C\downarrow(2)$ value of the second step is 205 K. Below 190 K, the $\chi_M T$ values remain approximately constant. Upon heating, the $\chi_M T$ values increase rapidly between 200 and 250 K to attain a broad plateau at 1.80 $cm^3 K mol^{-1}$. Here, the $\chi_M T$ values consequently lie lower than the values of the cooling mode. The $T_C\uparrow(2)$ value of this step is 220 K. Between 250 and 295 K, the $\chi_M T$ values remain constant. Above 295 K, the $\chi_M T$ values increase rapidly to a maximum value of 3.20 $cm^3 K mol^{-1}$ at 320 K. The $T_C\uparrow(1)$ value of this step is 304 K, which results in a 50 K wide thermal hysteresis loop for the first step and 15 K for the second step. After the initial heating to 350 K, the hysteresis loop can be repeated several times. The varying curve progression for the first cycle and all following cycles can have different reasons. Obviously, the compound crystallises at room temperature in a mixed HS/LS state (approximately 60/40). Upon heating to 350 K, the transition curves are shifted to lower temperatures and now a complete two-step spin transition is observed. The most likely explanation for this observation is a (partial) loss of the included methanol at 350 K. In order to check this theory, a TG analysis of compound **5**·MeOH was performed and the results are given in the Supporting Information (Figure S1). Upon heating up to 348 K, approximately 60% of the included methanol is lost, and for a complete removal of the solvent, heating above 373 K is necessary. Consequently, further heating of the SQUID sample to 400 K results in a complete loss of the crystal solvent, and a pure HS compound is obtained as for the separately prepared powder sample. These solvent effects are entirely contrary to the effects observed for the pair **6**/**6**·0.25MeOH, where the solvent-free compound **6** shows a complete SCO, while the methanol-containing compound **6**·0.25MeOH is always HS.[14]

Solvent effects are well known for SCO compounds, and a similar dependence can be observed for the other chain compounds in this study. For **2**·MeOH, upon heating to 400 K for 60 min, the included solvent is removed, and the transition temperature is shifted to lower temperatures (from 168 K to 115 K) accompanied with the appearance of a 10 K wide hysteresis loop ($T_{1/2}\downarrow$ = 110 K, $T_{1/2}\uparrow$ = 120 K). As a consequence, the second step of the spin transition is shifted from 91 K to a temperature somewhere below 80 K and is now kinetically trapped. This becomes obvious in the heating mode of the susceptibility measurements of the tempered sample (**2**). A descent in the $\chi_M T$ value at 80 K is obtained when keeping the temperature constant for 60 min while the susceptibility was recorded every 5 min. As a result, the $\chi_M T$ values at 80 K drop over this period of time from 1.78 $cm^3 K mol^{-1}$ down to 1.38 $cm^3 K mol^{-1}$. In the case of **2**·EtOH ($T_{1/2}$ = 116 K, no hysteresis), the transition temperature does not change significantly upon the loss of ethanol, and a 10 K wide thermal hysteresis loop is observed as for the tempered methanol sample (**2**). In contrast to this, the transition temperature of the first step of **4** (high-temperature step) is shifted to higher temperatures when going from the crystalline sample **4**·0.25MeOH to the solvent-free powder sample **4**. This indicates that, in general, the influence of solvent effects on the SCO behaviour is difficult to predict without any further (structural) information. A strong dependence of the spin-transition behaviour on included solvent molecules is also observed for the different compounds of **3**. The gradual incomplete spin transition of the solvent-free powder sample **3** can be explained with the absence of significant interchain interactions. This example demonstrates that interchain interactions are important for the observation of cooperative effects, as already suggested for compound **6**.[14] For the two crystalline samples, a similar transition temperature is obtained, but the thermal hysteresis loop is more pronounced for **3**·MeOH (27 K, $T_C\downarrow$ = 155 K, $T_C\uparrow$ = 182 K) relative to **3**·1.5Tol (4 K, $T_{1/2}\downarrow$ = 165 K, $T_{1/2}\uparrow$ = 169 K). Additionally, the spin transition of **3**·MeOH is a complete one-step transition, while for **3**·1.5Tol it stops at $\gamma_{HS} \approx 0.5$.

X-ray Structure Analysis

Full single-crystal X-ray diffraction structure and refinement details have been obtained for the compounds $\mathbf{1}^{HS}$, $\mathbf{1}^{HS-LS}$, $\mathbf{2}^{HS}$·MeOH, $\mathbf{2}^{HS-LS}$·MeOH, $\mathbf{3}^{HS}$·MeOH, $\mathbf{3}^{HS}$·1.5Tol, $\mathbf{4}^{HS}$·0.25MeOH, $\mathbf{4}^{LS}$·0.25MeOH and $\mathbf{5}^{LS/LS}$·MeOH. In the case of **4**·0.25MeOH, it was possible to determine the structure in the HS and LS states. For compounds **1**, **2**·MeOH and **3**·1.5Tol (because of the low measurement quality of $\mathbf{3}^{HS-LS}$·1.5Tol, the crystal structure can only be seen as a motif), it was possible to determine the molecule structure at $\gamma_{HS} \approx 0.5$, in order to more clearly evaluate the reasons for the step in the transition curve. In the case of compound **3**·MeOH, the crystals crumbled while cooling down. The motif of the X-ray structure of $\mathbf{6}^{HS}$·0.25MeOH was reported previously.[14] The crystallographic data and refinement details are summarised in Tables 5 and 6. Selected bond lengths and angles within the first coordination sphere of the iron centre are summarised in Table 2. ORTEP drawings of the asymmetric units of the compounds are given in Figure 2.

In all complexes the iron(II) centres are located in distorted octahedral coordination spheres consisting of one equatorially coordinated tetradentate Schiff base like ligand and two axially coordinated bis(monodentate) bridging ligands (bppa, bpea, bipy), bound through terminal 4-pyridyl

Table 2. Selected bond lengths [Å] and angles [°] within the first coordination sphere of the iron(II) complexes discussed in this work with spin state *S* at temperature *T*.

Compound	*T* / K	*S*	Fe–N1/2	Fe–O1/2	Fe–L_{ax}	O1–Fe–O2	L_{ax}–Fe–L_{ax}
1	200	2	2.091(2)/2.083(3)	1.998(2)/2.012(2)	2.253(3)/2.301(3)[d]	107.47(9)	177.82(8)[d]
	100	2	2.078(3)/2.073(2)	1.994(2)/2.007(2)	2.236(3)/2.283(3)	106.92(8)	177.11(9)
		0	1.902(2)/1.908(3)	1.920(2)/1.944(2)	2.000(2)[e]/2.011(2)	89.09(9)	178.06(10)[e]
2·MeOH	225	2	2.081(2)/2.098(2)	2.013(2)/2.011(1)	2.266(2)/2.239(2)	109.64(6)	173.42(7)
	125	2	2.066(3)/2.075(3)	2.004(2)/2.008(2)	2.238(3)/2.221(3)	107.70(10)	172.64(11)
		0	1.912(3)/1.919(3)	1.948(2)/1.948(2)	1.996(3)[f]/2.035(3)	92.09(9)	174.55(11)[f]
3·1.5Tol	200	2	2.094(4)/2.115(4)	2.034(3)/2.016(3)	2.218(4)[a]/2.285(5)[b]/2.291(3)[g]	110.98(13)	175.81(2)[a,g]/ 169.23(2)[b,g]
		2[c]	2.12/2.11	2.04/2.05	2.26/2.22	112.3	173.3
		0[c]	1.91/1.89	1.96/1.95	2.00/2.00	90.1	176.5
3·MeOH	200	2	2.102(2)/2.091(2)	2.013(2)/2.027(2)	2.279(2)/2.256(2)[h]	109.80(6)	174.29(7)[h]
4·0.25MeOH	293	2	2.087(2)/2.083(2)	1.997(2)/2.015(2)	2.259(2)/2.293(2)	109.85(7)	176.47(8)
	7	0	1.899(3)/1.892(2)	1.937(2)/1.937(3)	2.012(3)/2.032(3)	91.15(10)	176.86(10)
5·MeOH	175	0	1.903(3)/1.909(3)	1.926(3)/1.939(3)	1.992(4)/1.996(4)[i]	87.90(11)	176.49(12)[I]
	175	0	1.901(3)/1.898(3)	1.935(3)/1.939(3)	1.981(4)/2.009(4)[i]	88.07(11)	176.78(12)[i]

[a] Related to N(3A). [b] Related to N(3B). [c] Values taken from a structure motif as a result of low refinement quality. [d] Symmetry code: –1 + *x*, 1/2 – *y*, –1/2 + *z*. [e] Symmetry code: –1 + *x*, *y*, *z*. [f] Symmetry code: –1 + *x*, *y*, –1 + *z*. [g] Symmetry code: *x*, *y*, –1 + *z*. [h] Symmetry code: –1 + *x*, 1 + *y*, *z*. [i] Symmetry code: 1 + *x*, *y*, *z*.

groups. Each bridging ligand "connects" two iron(II) centres, which results in the formation of extended 1D chains as given in Figure 3. The average Fe–N/O bond lengths and angles are within the range reported previously for similar mononuclear,[13] binuclear[15] and polymer[14] HS and LS iron(II) complexes. For $\mathbf{3}^{HS}$·1.5Tol, one ethyl acetate side group of the equatorial ligand as well as one pyridyl ring of the axial ligand bpea are disordered.

The contents of the asymmetric units for all compounds, with the exception **5**·MeOH, are made up of one crystallographically distinct iron(II) centre, when either the pure HS or LS state is expected, according to the results of the magnetic measurements. For compound **5**·MeOH, two crystallographically distinct iron(II) centres with slightly different crystallographic environments can be found. In the range of the IP, the asymmetric units are doubled and contain two crystallographically distinct iron centres, of which one can be assigned to iron(II) in the HS state (Fe1) and one to iron(II) in the LS state (Fe2).

Compounds $\mathbf{1}^{HS}$ ($P2_1/c$) and $\mathbf{2}^{HS}$·MeOH ($C2/c$) crystallise in monoclinic space groups, and $\mathbf{3}^{HS}$·1.5Tol and $\mathbf{3}^{HS}$·MeOH in the triclinic space group $P\bar{1}$. For $\mathbf{1}^{HS–LS}$, $\mathbf{2}^{HS–LS}$·MeOH and $\mathbf{3}^{HS–LS}$·1.5Tol, the change in the spin state at the iron(II) centres upon cooling can easily be followed by observing the O–Fe–O angle, the so-called bite of the equatorial ligand, which changes upon spin transition from about 110° in the HS state to about 90° in the LS state. Moreover, a characteristic shortening (ca. 10%) of the bond lengths occurs within the first coordination sphere. There are two different reasons for the change in the size of the asymmetric unit: For $\mathbf{2}^{HS}$·MeOH, upon cooling to 125 K, the symmetry of the system is reduced from $C2/c$ to $P2_1/c$, half of the systematic extinctions observed at 225 K have vanished, as displayed in Figure 4. Consequently, the asymmetric unit of $\mathbf{2}^{HS–LS}$·MeOH consists of two crystallographically distinct iron(II) centres, as mentioned before. A one-dimensional chain of alternating HS and LS iron centres is formed as given in Figure 6. In contrast to this, at $\mathbf{1}^{HS}$ no change in the symmetry of the system is observed relative to $\mathbf{1}^{HS–LS}$, but an elongation of the unit cell along the *a* axis. Consequently, the cell volume is doubled from 3046(2) Å^3 at 200 K to 5947(3) Å^3 at 100 K. As in $\mathbf{2}^{HS–LS}$·MeOH, a chain of alternating HS and LS iron centres is formed. The latter case is also true for **3**·1.5Tol, as no symmetry change is observed, but a duplication of the cell volume [1966.5(4) Å^3 at 200 K to 3861.2(3) Å^3 at 130 K]. It should be noted that the disorder of the equatorial and axial ligand disappears upon reaching the IP. For compound **4**·0.25MeOH, it was possible to determine the X-ray structure in the HS and the LS states. In both cases, the compound crystallises in the triclinic space group $P\bar{1}$; unfortunately, we were not able to determine the X-ray structure at the plateau at 106 K. The bond lengths and angles around the iron(II) centre differ significantly at 298 and 7 K, highlighting the already discussed changes in spin state. Upon spin transition, the cell volume is reduced from 1427.8(5) Å^3 at 298 K to 1328.4(8) Å^3 at 7 K, and the density increases from 1.337 g cm^{-3} to 1.436 g cm^{-3}. By considering the additional contribution of the thermal contraction, the observed change in the cell volume ($\Delta V/V$ = 7.2%, ΔV = 49.7 Å^3/Fe) is in the range expected for an iron(II) SCO complex (contribution of the SCO itself: $\Delta V/V$ = 3.8–6%; ΔV = 25–35 Å^3/Fe).[1] Compound **5**·MeOH also crystallises in the triclinic space group $P\bar{1}$. The asymmetric unit of $\mathbf{5}^{LS/LS}$·MeOH at 175 K is made up of two crystallographically distinct iron(II) centres that are both in the LS state, but with slight geometrical differences within the inner coordination sphere caused by subtly different crystallographic environments of Fe1 and Fe2 as a result of incorporated solvent molecules. Crystallographically distinct iron centres are the most likely reason for the step in the transition curve.

The step in the transition curve of compound **1** and **2**·MeOH is clearly related to the formation of an alternating [HS–LS] chain, and this may also be the case for **3**·1.5Tol; however, the order/disorder transition has to be kept in

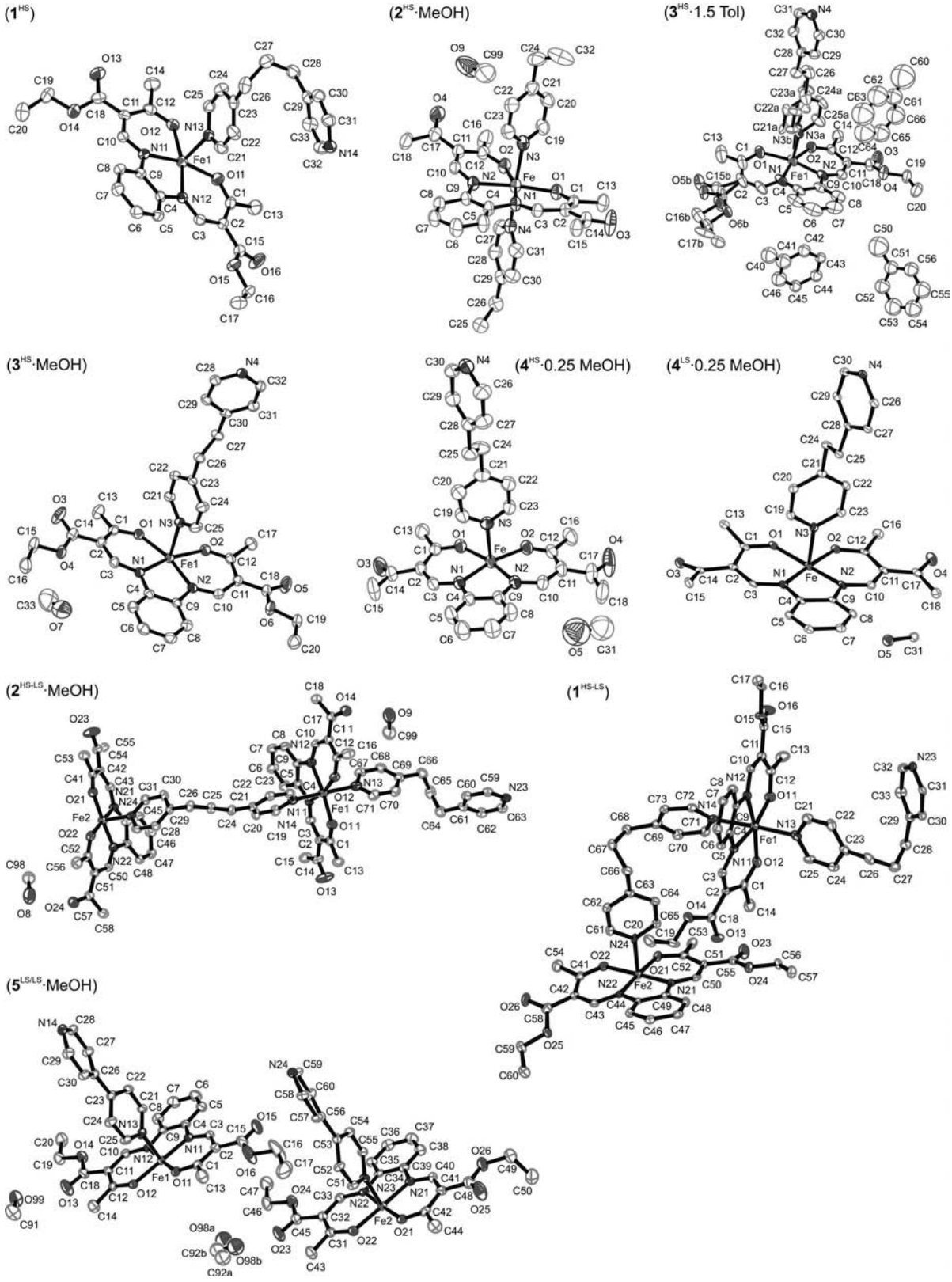

Figure 2. ORTEP drawing of the asymmetric units of the compounds discussed in this work, with the spin states of the iron(II) centres indicated at the top and the atom numbering scheme used in the text. The ellipsoids are shown with a 50% probability. Hydrogen atoms have been omitted for clarity.

mind. For **1** and **2**·MeOH, the iron centres are clearly crystallograpically equivalent in the HS state, while at the IP, two crystallographically distinct iron centres are obtained. This superstructure is only generated upon spin transition.

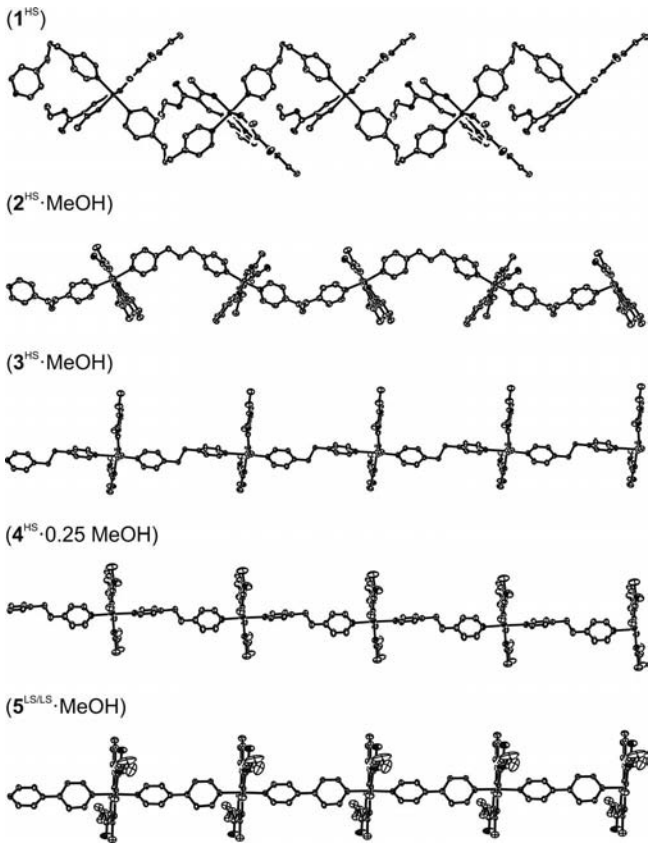

Figure 3. ORTEP drawing of the zigzag chain structure of compounds $\mathbf{1}^{HS}$ and $\mathbf{2}^{HS}$·MeOH with the axial bppa ligand, the steplike chain structure of $\mathbf{3}^{HS}$·MeOH and $\mathbf{4}^{HS}$·0.25MeOH with the bpea ligand and the linear chain structure of $\mathbf{5}^{LS/LS}$·MeOH with the bipy ligand.

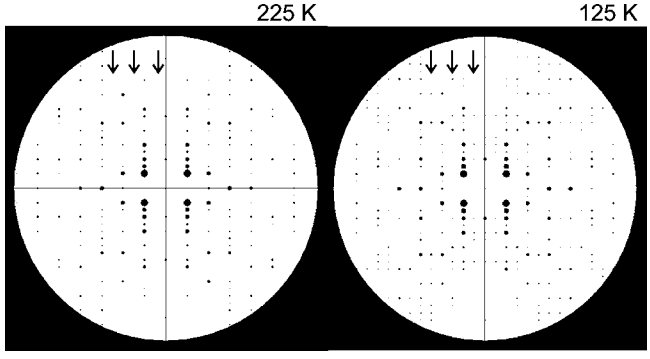

Figure 4. Reciprocal space [0 *k l*] section of compound **2**·MeOH at 225 and 125 K represented with the Layer Program.

Of the three already existing possibilities for the explanation of two-step spin transitions, two possibilities can be ruled out: The first one – two or more nonequivalent iron centres – can be excluded according to the results from X-ray structure analysis. The second possibility – the formation of energetically stable [HS–LS] pairs – is also not very likely. The formation of such pairs is associated with antiferromagnetic interactions between the neighbouring iron centres.[7] Results from magnetic measurements on polymer HS iron(II) compounds of this ligand type show that the magnetic exchange interaction along the polymer chain is negligible.[16] Hence, there is only the possibility of intermolecular interactions, generated through cooperative long-ranged (ferromagnetic-type) interactions or antiferromagnetic interactions between the HS and the LS sublattices. However, this model does not help us to define rules for the purposeful synthesis of 1D SCO materials with two-step spin transitions. Consequently, a new model is needed to explain the differences in the magnetic properties of the 1D chain compounds presented in this paper. A detailed comparison of intra- and interchain interactions is necessary to develop this model. Table 3 shows selected intra- and interchain distances between the iron centres. Table 4 summarises intermolecular hydrogen bonds and short contacts, whereas in the Supporting Information, Tables S2 and S3, a detailed list of intermolecular hydrogen bonds and short intermolecular contacts are given.

Table 3. Selected intra- (Fe···Fe) and interchain (Fe···Fe*) iron(II) distances [Å] of the coordination polymers discussed in this work.

Compound	*T* [K]	*S*	$Fe^{HS}\cdots Fe^{HS}$	$Fe^{LS}\cdots Fe^{LS}$	$Fe^{HS}\cdots Fe^{LS}$	Fe···Fe*
1	200	2	10.01	–	–	8.25
	100	2/0	–	–	9.91/10.06	–
2·MeOH	225	2	13.14/13.80	–	–	8.55
	125	2/0	–	–	12.95/13.58	–
3·1.5Tol	200	2	13.85	–	–	13.96
3·MeOH	200	2	13.88	–	–	10.22
4·0.25MeOH	293	2	13.83	–	–	8.68
	7	0	–	13.33	–	8.34
5·MeOH	175	0	–	11.10	–	7.56

In order to provide a better overview of the influence of packing effects on the spin-transition properties, in the following, the differences in the crystal packing are compared by pairs with the different axial ligands as sort key. The first pair of structures to be compared are the compounds with bppa as bridging ligand, namely **1** and **2**·MeOH (top of Figure 5). The infinite 1D chains of **1** propagate along [2 0 1] for $\mathbf{1}^{HS}$ and [1 0 0] for $\mathbf{1}^{HS-LS}$, a consequence from the symmetry change. The strong distortion of the axial bridging ligand results in the formation of zigzag chains. Between adjacent chains there is a multitude of short interactions, mainly between the ethyl acetate side groups of the equatorial ligand and the CH groups of the axial ligand. Accompanied with the SCO, a change in the intrachain Fe···Fe separation distance can be observed. One could expect this to be due to the decrease in the Fe–L_{ax} distances from HS to LS. Along the [HS–HS] chain of $\mathbf{1}^{HS}$, a Fe···Fe separation distance of 10.01 Å can be found, which changes upon spin transition to the IP along $\mathbf{1}^{HS-LS}$ alternately to 9.91 Å and 10.06 Å. Surprisingly, a shortening of the $Fe^{HS}\cdots Fe^{LS}$ separation distance can only be seen for one chain link, whereas the other is elongated, although at every second iron centre, the Fe–L_{ax} bond lengths decrease. A closer look reveals that the end-to-end distances of the strongly twisted bppa ligands elongate significantly from 6.98 Å at $\mathbf{1}^{HS}$ to 7.06/7.27 Å at $\mathbf{1}^{HS-LS}$. The bppa ligand can be thought to "compensate" the shortening of the

Table 4. Summary of intermolecular contacts per iron centre of the iron(II) coordination polymers discussed in this work. The number of contacts to solvent molecules is given in parentheses. For details on the hydrogen bonds with d(D···A) < R(D) + R(A) + 0.50 Å, d(H···A) < R(H) + R(A)–0.12 Å, D–H···A >100.0° see Supporting Information, Table S2; for details on the short contacts with Δ = d(I···J) – [R(I) + R(J)] (sum of the van der Waals radii) see Supporting Information, Table S3.

	H Bond	Δ >0.2 [Å]	Δ = 0.2–0.1 [Å]	Δ <0.1 [Å]	Σ (solvent)
$\mathbf{1}^{HS}$	2		2	6	10
$\mathbf{1}^{HS–LS}$	3		2	8.5	13.5
$\mathbf{2}^{HS}$·MeOH	(2)		1	4	5 (2)
$\mathbf{2}^{HS–LS}$·MeOH	(2)	0.5	3	9	12.5 (2)
$\mathbf{3}^{HS}$·1.5Tol	4		1 (1)	1 (1)	6 (2)
$\mathbf{3}^{HS}$·MeOH	3 (1)	1	2	9	15 (1)
$\mathbf{4}^{HS}$·0.25MeOH	2	(1)	3 (3)	3 (3)	8 (7)
$\mathbf{4}^{LS}$·0.25MeOH	2	(1)	2 (2)	12 (2)	16 (5)
5·MeOH[a]	2/1/0 (3)	0/0/1 (2)	3/0/1(2)	2/4/1 (9)	7/5/3 (16)

[a] Distinguished between Fe1–Fe1/Fe2–Fe2/Fe1–Fe2 interactions and contacts to the solvent (MeOH).

Fe–L_{ax} distances, so that on average the chain length remains the same. The relative position of the iron centres and the equatorial ligands does not change, possibly because of the restraining interactions caused by the short contacts given in Table 4. The infinite 1D chains of **2**·MeOH (HS and LS) propagate along the [1 0 1] direction. The distortion of the axial bridging ligand results also in the formation of zigzag chains, but with an angle of about 56° between the planes of neighbouring equatorial ligands, the distortion is weaker than in **1**. Between the hydroxy hydrogen atom (H9) of the methanol molecule and the oxygen atom (O4) of one acetyl side group of the equatorial ligand, a hydrogen bond is formed. This is only of indirect importance; however, the oxygen atom as a strong H-bond acceptor is "occupied" and cannot form any kind of interchain interaction. Furthermore a number of weak van

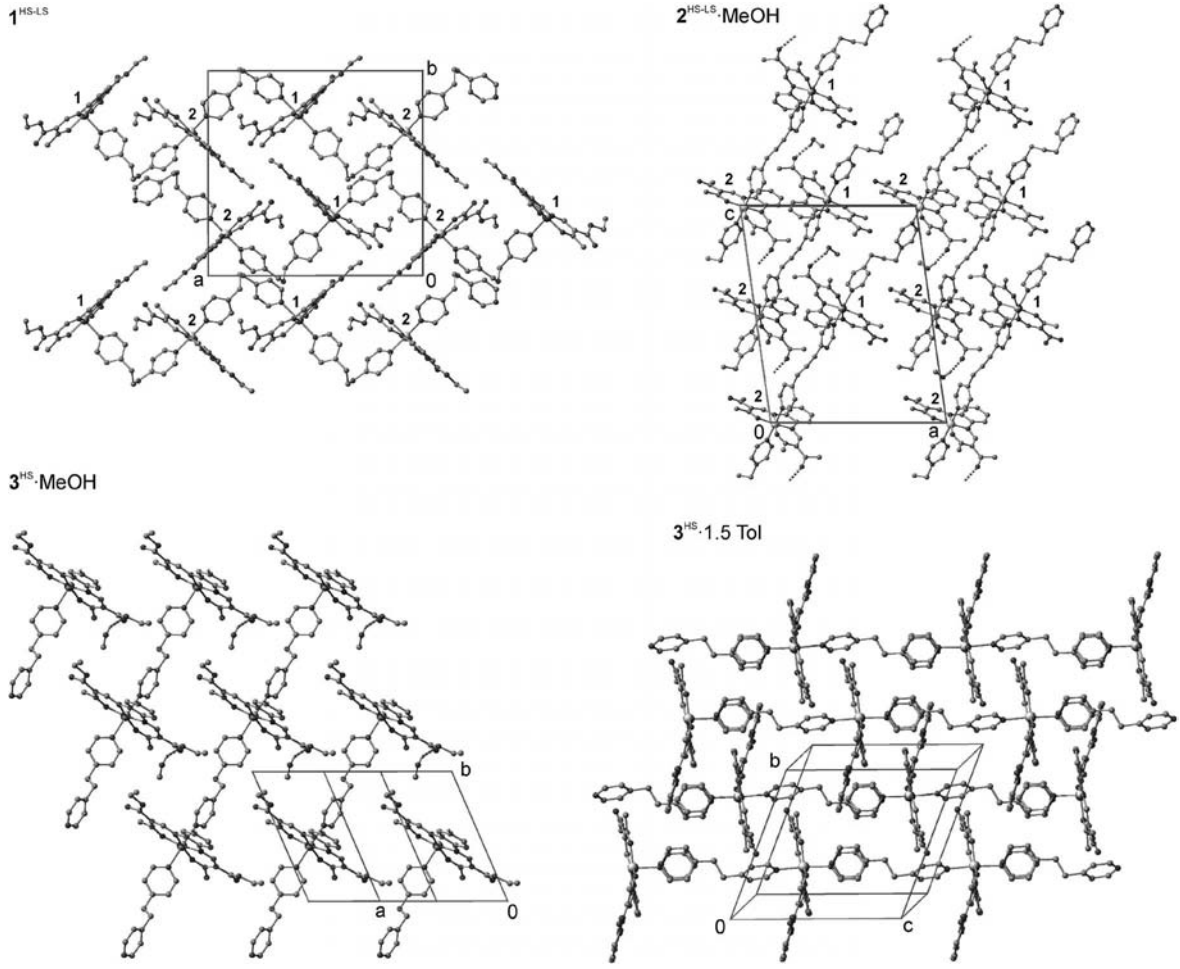

Figure 5. Plot of the crystal packing of the iron(II) coordination polymers **1**, **2**·MeOH, **3**·1.5Tol and **3**·MeOH. 1 and 2 refer to the different iron centres in the HS/LS states. Hydrogen bonds are shown as dashed lines. Hydrogen atoms are omitted for clarity.

der Waals contacts occur, mainly involving the second acetyl oxygen atom (O3), the methanol hydroxy oxygen atom (O9) and CH groups of the axial ligand. In the HS state, all hydrogen bonds are mediated by the methanol molecule, while in the HS/LS state, one additional direct contact is observed (see Table 4). By looking at the intrachain Fe···Fe separation distance, another situation can be observed for compound **2**·MeOH relative to **1**. Two differently elongated chain links can be found in $\mathbf{2}^{HS}$·MeOH (13.14 and 13.80 Å), which change significantly to 12.95 and 13.58 Å in $\mathbf{2}^{HS-LS}$·MeOH on the IP. The changes in the end-to-end distances of the bppa ligands (Δ = 0.04 and 0.06 Å) are not as pronounced as observed for compound **1**, thus the shortening of the Fe–L_{ax} distances are only marginally compensated. The more pronounced zigzag chain in the case of **1**, in combination with the sterically more-demanding equatorial ligand L1 and the more direct (not mediated over the included methanol molecule) interchain interactions, results in the fact that the single chains of **1** are more strongly wedged together than in **2**·MeOH, as illustrated in Figure 5. Thus, the changes in the bond lengths expected upon spin transition cannot be as easily followed for **1** relative to **2**·MeOH, and the spin-transition behaviour changes from a complete two-step transition (**2**·MeOH) to an incomplete spin transition for **1** that stops at the IP.

The infinite 1D chains of **3**·MeOH and **3**·1.5Tol have the base vectors [1 $\bar{1}$ 0] and [0 0 1], respectively (Figure 5, bottom). Because of the less-flexible ethyl bridge of the axial ligand bpea (instead of the propyl bridge of bppa), a stepped chain structure is observed for both compounds compared to the zigzag structure mentioned above. The intrachain Fe···Fe separation distances are almost identical: 13.88 (**3**·MeOH) and 13.85 Å (**3**·1.5Tol). The methanol molecule of **3**·MeOH is hydrogen bonded to one ethoxy oxygen atom (O4) of the equatorial ligand. The other carboxylate oxygen atoms and carbonyl oxygen atoms of the equatorial ligand form weak interactions with the CH groups of the axial ligand of adjacent chains. These interactions together with the other short contacts are the most likely explanation for the 27 K wide hysteresis loop in this compound. The molecule packing of **3**·1.5Tol has a lower density than that in **3**·MeOH (1.291 relative to 1.363 g cm^{-3}), possibly because of the relatively huge disordered toluene molecules incorporated between the chains. This can also be seen by comparing the interchain Fe···Fe* separation distances (Fe* is the iron centre generated through the symmetry operation *–x*, *–y*, *–z*), which are significantly longer in **3**·1.5Tol (13.96 relative to 10.22 Å). Consequently, only a few interchain interactions can be found (see Table 4), mainly between both carbonyl oxygen atoms of the equatorial ligand and the carbon-bonded hydrogen atoms of the axial ligand bpea. This satisfactorily explains the reduction in the hysteresis width when going from the methanol- to the toluene-containing sample. This pair also illustrates that it is important to compare all intermolecular contacts, as the number of hydrogen bonds is the same for both compounds. However, no explanation for the IP of **3**·1.5Tol can be derived from the crystal packing, as was possible for **1** and **2**·MeOH. Therefore, it can be assumed that the disorder observed in the HS structure is responsible for the incomplete spin transition with only 50% of the iron centres involved. The infinite 1D chains of **4**·0.25MeOH (HS and LS) propagate along [1 $\bar{1}$ 0] with the same stepped structure observed for compounds **3**·MeOH and **3**·1.5Tol. Upon spin transition, the intrachain Fe···Fe distance is shortened by about 0.50 Å, whereas the end-to-end distance of the axial bpea ligand is only shortened by about 0.01 Å, which highlights the stiffness of bpea. In comparison with compound **3**, the solvent molecule seems to influence the SCO behaviour of compound **4** in a similar way, because, for both examples, the loss of methanol is accompanied with a decrease in the cooperativity when comparing the solvent-containing and the solvent-free sample. In contrast to compound **3**·MeOH with its full occupancy methanol molecule involved in strong hydrogen bonds, the structure of **4**·0.25MeOH only contains a quarter occupancy methanol, which is furthermore not hydrogen bonded to one of the carbonyl oxygen atoms of the equatorial ligand. Therefore, both acetyl oxygen atoms of the equatorial ligand form nonclassical hydrogen bonds to adjacent chains involving the CH groups of the axial ligand, which explains the observed hysteresis loop, and are probably also responsible for the small IP in the heating mode.

The molecular structure of $\mathbf{5}^{LS/LS}$·MeOH was determined at 175 K, thus all iron(II) centres are in the LS state. Because of the slightly different chemical surroundings as a result of an additional disordered methanol molecule, two complex molecules with nonequivalent iron(II) sites can be found in the asymmetric unit. The infinite 1D chains of compound **5**·MeOH run along [1 0 0] and are totally linear because of the bridging ligand bipy. Adjacent chains are arranged in a way that the ethyl acetate side groups of the equatorial ligand point to each other. Consequently, many short intermolecular interactions can be observed. Every methanol molecule forms a hydrogen bond to a carboxylate oxygen atom of one of the equatorial ligands. However, whereas for Fe1, typical hydrogen bond values are found (H99···O13: 1.95 Å, see Table 4); in the case of Fe2, a significantly weaker hydrogen bond is observed (H98b···O23: 2.32 Å, Table 4) and, additionally, the methanol molecule is disordered. This supports the results from the magnetic measurements and TG analysis, that, upon heating to 350 K, only one of the two methanol molecules is lost and two crystallographically different iron centres are obtained, which undergo spin transition at different temperatures. Short interactions are also observed between the remaining carboxylate oxygen atoms and CH groups of the axial ligand and the acetyl CH_3 groups of adjacent chains, as summarised in Table 4. In the magnetic measurements, different widths are observed for the two hysteresis loops, and the question arises whether this is reflected in the X-ray structure. In Figure 6, a top view of the packing of the chains in the crystal is given. The 1D chains of equivalent iron centres form layers along the *c* axis that alternate along the *b* axis. The summary of the intermolecular interactions given in Table 4 reveals that, between the chains of Fe1,

more and shorter contacts are observed relative to the Fe2–Fe2 interactions. Between the layers (Fe1–Fe2 interactions), even fewer contacts are observed. Thus, the different hysteresis widths can be explained by differences in the number and strength of interchain contacts.

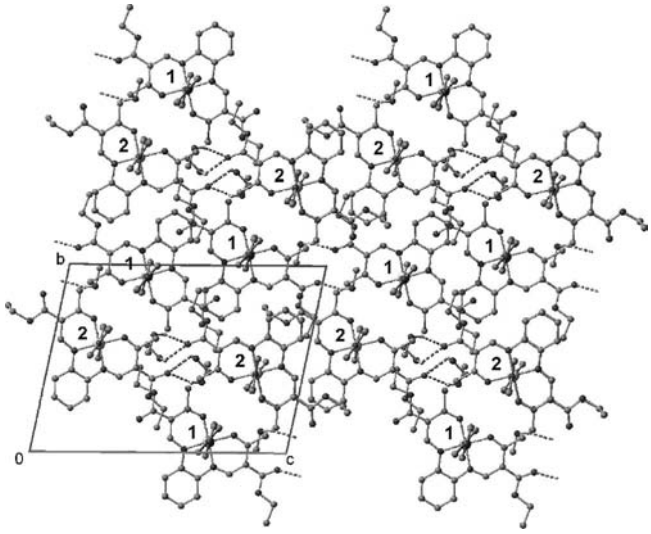

Figure 6. Top view of the crystal packing of the iron(II) coordination polymer **5**·MeOH. Hydrogen bonds shown as dashed lines. Hydrogen atoms are omitted for clarity. 1 and 2 refer to the different iron centres in the HS/LS states.

Investigations in Solution By Using ^{1}H NMR Spectroscopy

Variable-temperature NMR spectroscopy is a valuable tool to follow a spin transition in solution by interpretation of the temperature dependence of the ^{1}H NMR chemical shifts.[15b] In order to prove the influence of the intermolecular interactions on the transition temperature and the appearance of a step during a SCO, compounds **1** and **3**·1.5Tol were dissolved in [D_8]toluene, as, in solution, all packing effects are switched off. For all other compounds, the solubility in toluene was too low for measurement by this method and another solvent with similar properties (liquid range, non-coordinating) was not available. Before starting temperature-dependent measurements, it was important to verify that all iron centres retain their octahedral coordination sphere, and, therefore, the 1D coordination polymer is intact in solution. This could be confirmed by the signal assignment, which is shown in Figure 7. The resonances of the equatorial ligand L1 appear in a similar region as reported previously for mononuclear iron(II) complexes of this ligand with different axial ligands (pyridine[15b] and 4-cyanopyridine[13c]). The signals are therefore assigned to the CH_3 group (a) and the ethyl group (b, c) of the substituents of the equatorial ligand. The signal at about 10 ppm with a relative intensity of 1 is assigned to the proton (d) of the phenlyene ring. The signals of the two remaining protons of the equatorial ligand are not assigned. By considering the NMR spectra of this type of complex in pyridine,[15b] the HC–N proton signal should be in the 400–500 ppm region of the spectrum, but it is very broad and therefore difficult to detect. The signal for the second proton of the phenylene ring is probably in the –5 to 5 ppm region of the spectrum, but is too broad to be detected because of additional signals from the solvent, impurities and the axial ligand. In each of the NMR spectra of **1** and **3**, in Figure 7, three remaining signals are observed, which belong to the axial ligands bppa and bpea. By assuming a chain structure, the bridging ligand bppa has a mirror plane in C26/C32, and four different signals are expected with the relative intensities of 2:2:2:1. If a *penta*-coordinated complex were to be considered (polymeric chain broken into monomers), seven different signals would be expected, each with the relative intensity of 1. As the chemical shift is strongly influenced by the paramagnetic iron centre, and this influence decreases rapidly with increasing distance from the metal centre (number of bonds), many of the signals would be expected in the diamagnetic region. In the case of complete dissociation, all the signals of the axial ligand would be expected in the diamagnetic region, which is not the case. As for the remaining signals, a relative intensity of 2 is observed, which clearly proves the polymeric chain structure of the complex in solution. With regard to the different line widths, the signal g with the smallest line width is assigned to the CH_2 group farthest away from the paramagnetic centre, and signals e and f are assigned to the

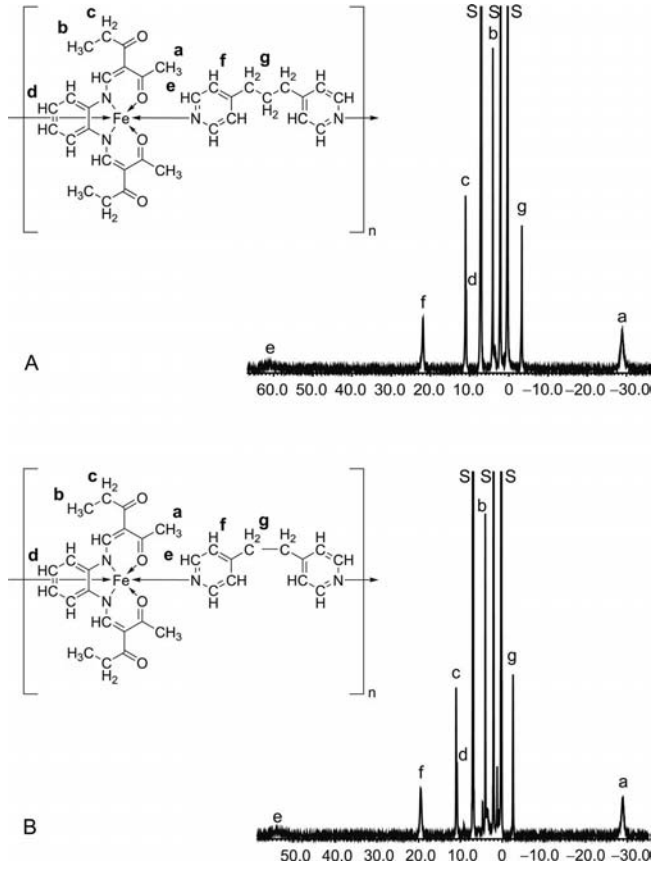

Figure 7. ^{1}H NMR spectra and signal assignment for complex (A) **1** and (B) **3** in [D_8]toluene at 75 °C (348 K).

proton *ortho* (e) and *meta* (f) to the pyridine nitrogen. The last signal (C26/32) could not be assigned, probably because it is too weak and in the diamagnetic region of the spectrum. The same observation can be made for chain complex **3**. Here, only three signals with the relative intensities 2:2:2 are expected, by assuming an octahedral complex, as observed in the NMR spectra. The resonances appear in a similar region to those for the bppa ligand and are thus assigned the same way as shown in Figure 7.

Figure 8 illustrates the shift in the NMR signals with temperature for complex **1**. In Figure 9, the isotropic shifts of the protons of the equatorial ligand are plotted vs. inverse temperature (Curie plot) for both complexes. Starting at 85 °C (358 K), upon cooling, the NMR signals are shifted to the more paramagnetic regions of the spectra, thus showing Curie behaviour. This is confirmed by the nearly linear temperature dependence seen in the Curie plots in the high-temperature region ($T > 285$ K, $1/T < 3.5 \times 10^3$ K^{-1}). This behaviour is similar to that expected for pure HS complexes. Below this point, the isotropic shift tends to zero, which indicates the start of the spin transition, as reported previously for this type of SCO complex with pyridine as axial ligands.[15b] From the ^{1}H signals of the NMR spectra shown in Figure 8, only signals a–d, f and g can be observed over the whole temperature range investigated. Of those signals, only the chemical shifts of signals a–d, which are assigned to the equatorial ligand, show the described behaviour. The temperature dependence of the chemical shifts of signals f and g, which are assigned to the axial ligand, is different; especially, in the high-temperature region, no Curie behaviour is observed. The most likely reason for this is the possibility of the axial ligand to rotate freely around the *z* axis. Attempts to analyse this behaviour by using the temperature-dependent fitting program (TDF), applied successfully for the mononuclear complexes,[15b] were not fruitful, and those resonances are not considered in the further discussion.

By assuming Curie behaviour for the high-spin species, the isotropic shift multiplied by the temperature is constant as long as the spin state does not change. A normalised plot of $\delta_{iso} \times T$ vs. T therefore reflects the high-spin mol fraction (γ_{HS}) of the complex as a function of temperature. In Figure 10, the transition curves of the averaged signals obtained in solution are compared with the results of the SQUID measurements in the solid state for both compounds. Because of the low solubility of both compounds at low temperature, only the beginning of the spin transition in solution could be detected by this method. Nevertheless, some trends can be observed as can be seen in Figure 10. When the transition curves of **1** and **3** obtained in solution are compared, both complexes show a gradual spin transition starting at similar temperatures of about 300 K. In the case of **1**, no indications for an abrupt SCO resting on a step as observed for the solid state analogue can be found. In comparison to the corresponding solid compounds (**1**, $T_{1/2}$ = 165 K; **3**·1.5Tol, $T_{1/2}$ = 123 K), the transition temperatures obtained in solution are clearly shifted to higher temperatures. These huge differences in SCO behaviour illustrate that the extent of cooperative interactions, as well as the transition temperature, is significantly influenced by packing effects.

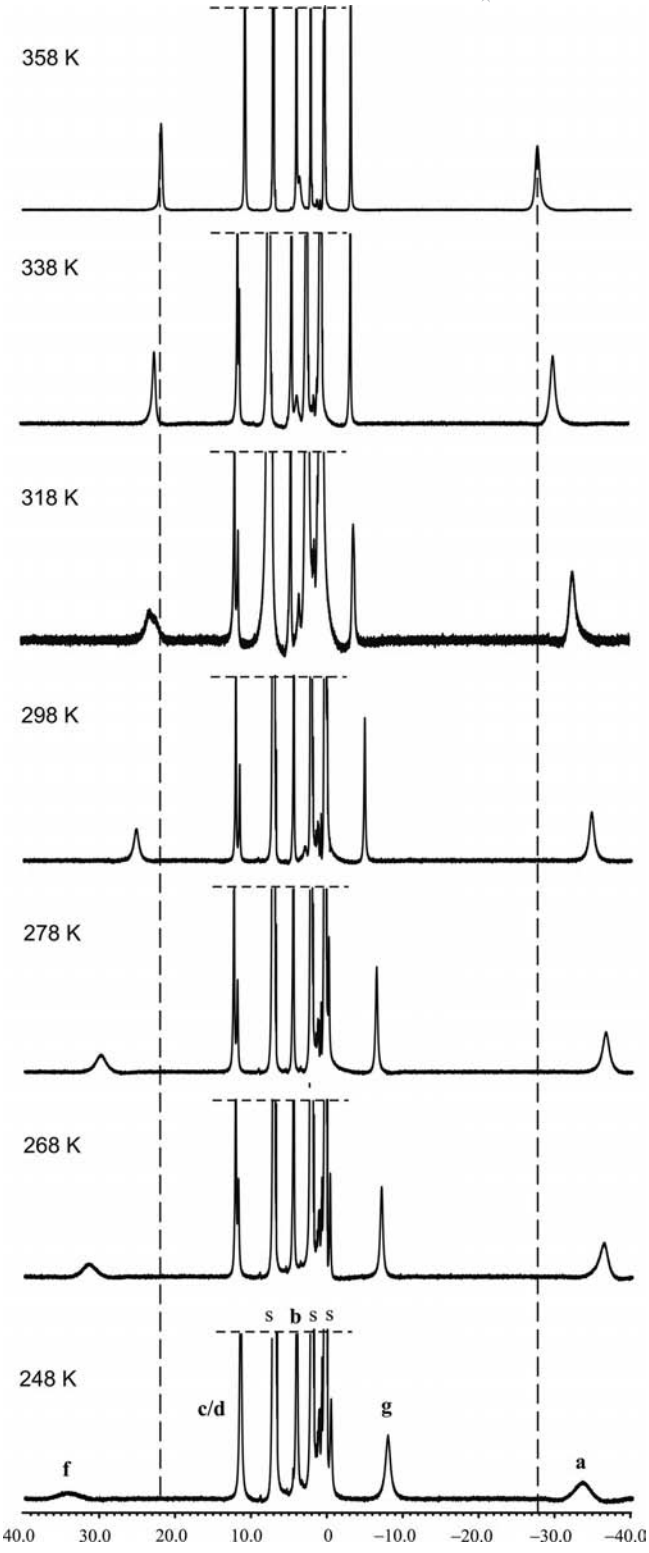

Figure 8. Temperature dependence of the chemical shifts of the signals a–d of complex **1**. The relative position of the resonance of signals a and f at 85 °C (358 K) is tagged with a line to more clearly illustrate the *T*-dependent shift of the signal.

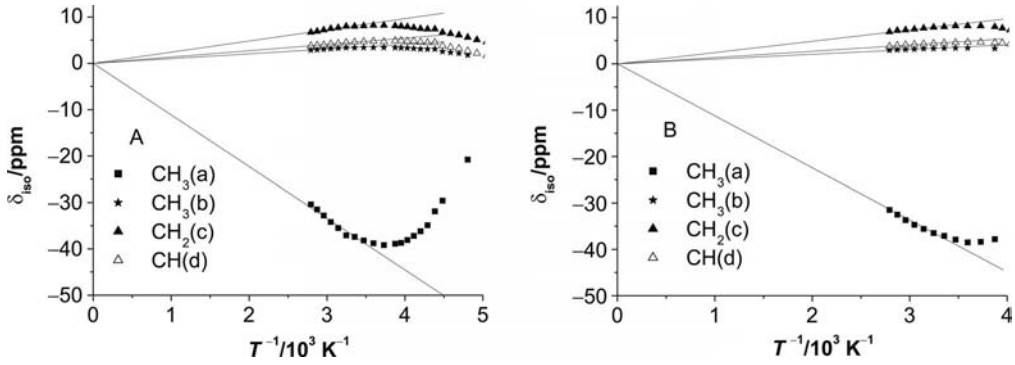

Figure 9. Chemical shifts δ_{iso} of complex **1** (A) and **3** (B) plotted vs. inverse temperature.

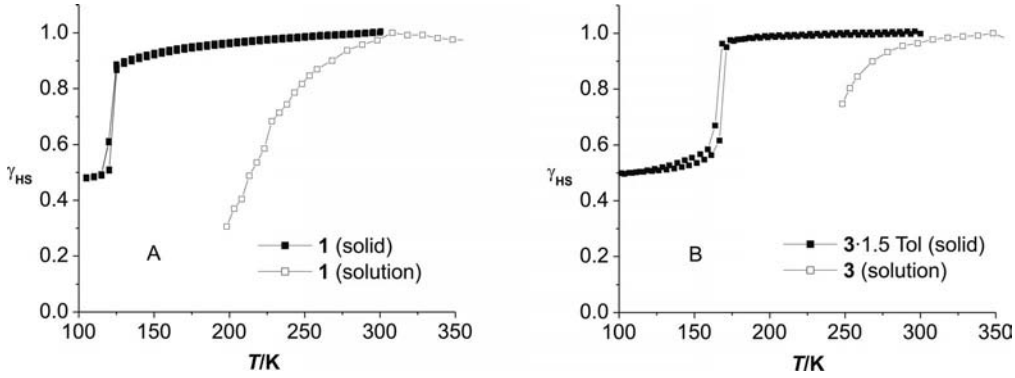

Figure 10. HS molar fraction γ_{HS} vs. T for complex **1** (A) and **3** (B) followed in solution and in the solid state.

Discussion

Different types of spin transition were obtained for the 13 compounds discussed in this work going from complete SCO to two-step SCO to incomplete SCO resting at the IP. In the same way, the cooperative interactions vary from gradual spin transition to up to 50 K wide thermal hysteresis loops. Some correlation can be found between the used axial bridging ligand, the width of the IP and the thermal hysteresis loop.

The width of the thermal hysteresis loop increases in the order bppa < bpea < bipy for both equatorial ligands (L1: 0 K, 4 K, 58 K; L2: 10 K, 22 K, 18 K, always highest values considered). The occurrence of a thermal hysteresis loop correlates well with the flexibility of the used bridging ligand and the number of interchain contacts, especially weak hydrogen bonds. For the more rigid ligand 4,4′-bipyridine, wide thermal hysteresis loops are observed, while the flexible bppa ligand only leads to stepped transitions or small thermal hysteresis loops. This is in agreement with literature results where 1D chains with iron(II) ions linked by loose bridges [e.g. bis(tetrazole) bridges with flexible spacers[17]] or ridged linkers without significant intermolecular interactions (bpea,[18] bipy,[19] dicyanamide[20]) result in gradual SCO behaviour. Combinations of intermolecular and intramolecular interactions contribute to the cooperative mechanisms during the spin transition and thus wide hysteresis loops. It is important to note that a combination of both interaction pathways is necessary to observe wide hysteresis loops. On the one hand, ridged linkers with no significant intermolecular interactions result in gradual spin transitions. On the other hand, if the number of intermolecular contacts is in the same order of magnitude, as for the examples presented in this work, the more ridged linkers lead to wider hysteresis loops. This is in agreement with the analytical solution of 1D systems where width and shape of the hysteresis loop depends on the balance between long- and short-range interactions.[21]

In the case of two-step or incomplete spin transitions, two different reasons have to be distinguished. For **3**·1.5Tol and **5**·MeOH, crystallograpically nonequivalent iron centres are clearly responsible for the incomplete/two-step spin transition. This is not the case for the other examples. Here, the width of the plateau $[T_{1/2}(1) - T_{1/2}(2)]$ decreases in the order bipy < bpea < bppa (L2: 0 K, 18 K, 77 K; L1: incomplete or disorder). With regard to the plateau in the transition curve, an interesting model was recently proposed by Koudriavtsev et al. for monomer complexes that can be transferred to our polymer systems. This quasi-chemical model uses specific molecular interactions for the description of stepwise or incomplete spin transitions for mononuclear complexes.[22] A HS → LS transition in a pair of HS molecules with attractively interacting ligands (e.g. hydrogen bonds) involves a relocation of the ligands towards the smaller LS molecule. If the Fe···Fe distances do not follow exactly the changes in Fe–L bonds in the LS species, then

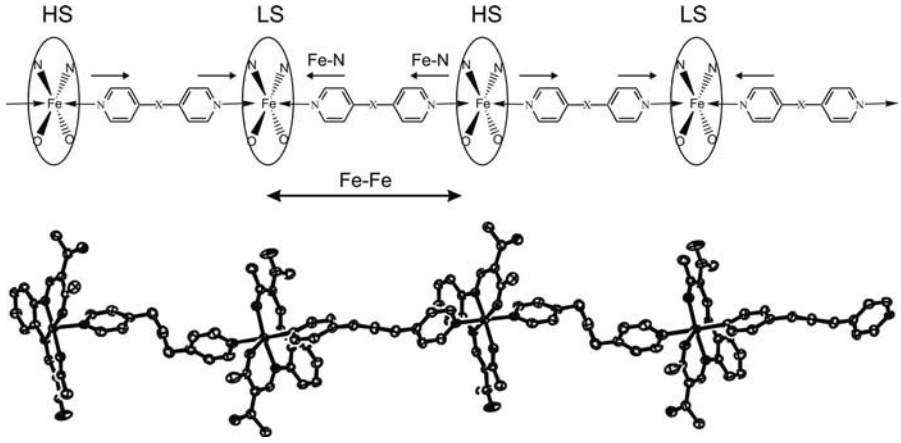

Figure 11. Schematic illustration of the model proposed for the spin transitions.

the corresponding bond in the HS partner is elongated and the HS state is thus stabilised.[21] This principle can be very easily transferred to polymer chain compounds, and the remaining question is why some of the compounds have one-step and others have two-step spin transitions; or in other words, are there factors that determine whether the Fe···Fe distances can follow exactly the changes in Fe–L bonds or not. The pair **1** and **2**·MeOH gives an indication of which factors inhibit a change in the Fe···Fe separation distance: a pronounced zigzag chain in combination with a number of interchain contacts results in an incomplete SCO for **1**. In the case of **2**·MeOH, the zigzag motive is less pronounced and less interchain contacts are observed, thus the second step can be observed. An even smaller step is observed for **4**·0.25MeOH – the chain is nearly linear, the number of interchain contacts does not change significantly, and for the linear chain compound **6**, no steps in the transition curve are observed, although there are several interchain contacts that are responsible for the thermal hysteresis loop. Thus, a pronounced zigzag structure of the 1D chain in combination with several interchain contacts result in stepwise spin transitions, even if all iron centres are equivalent in the HS state. In Figure 11, a schematic illustration of the proposed model is given.

Conclusion

The synthesis and characterisation of several new 1D chain iron(II) spin crossover compounds is described in this paper. A comparison of the spin-transition behaviour and the results from X-ray structure analysis lead to two conclusions for the rational design of spin-crossover materials. The first, and to some extent already discussed, theory is that a combination of intermolecular and intramolecular interactions contributes to the cooperative mechanisms during the spin transition and thus to the wide hysteresis loops. The second hypothesis is that a pronounced zigzag structure of the 1D chain in combination with several interchain contacts result in stepwise spins transitions, even if all iron centres are equivalent in the HS state. Further examples and further ongoing experiments, including photomagnetic investigations, DSC measurements and Mössbauer spectroscopy, are necessary to prove this theory. This work is already in progress and will be part of a subsequent publication.

Experimental Section

Magnetic Measurements: Magnetic susceptibility data were collected by using a Quantum Design MPMSR-2 SQUID magnetometer under an applied field of 0.5 T over the temperature range 2–350 K in the settle mode. The samples were placed in gelatine capsules held within a plastic straw. The data were corrected for the diamagnetic magnetisation of the ligands, using tabulated Pascal's constants, and of the sample holder. The measurements were analysed by using the CGS system.

NMR Spectroscopy: [D_8]toluene (D, 99.6%) was purchased from Euriso-top. The solvent was degassed with argon and stored over molecular sieves. The NMR samples were prepared under argon by using Schlenk techniques and locally made sealing equipment. Saturated solutions of the iron(II) complexes were prepared and stored in sealed or air-tight 5-mm NMR tubes. The NMR spectra were recorded on a JEOL EX 400e spectrometer operating at 400.182 MHz equipped with a variable-temperature unit over the temperature range –75 to +85 °C (198–358 K).

X-ray Structure Determination: The intensity data were collected on an Oxford XCalibur diffractometer (**1**, **3**·MeOH), a Nonius Kappa CCD diffractometer (**2**·MeOH, **3**·1.5Tol, **5**·MeOH) and a Huber 4-circle diffractometer (**4**·0.25MeOH) by using graphite-monochromated Mo-K_α radiation. The data were corrected for Lorentz and polarisation effects. The structures were solved by direct methods (SIR 97)[23] and refined by full-matrix least-square techniques against F_0^2 (SHELXL-97).[24] The hydrogen atoms were included at calculated positions with fixed displacement parameters. ORTEP-III[25] was used for the structure representation, SCHAKAL-99[26] to illustrate molecule packing. The crystallographic data are summarised in Tables 5 and 6. The quality of the data of **3**·1.5Tol in the mixed high-spin/low-spin state is inferior. We will therefore only be publishing the conformation of the molecule and the crystallographic data. CCDC-793143 ($\mathbf{1}^{HS}$), CCDC -793144 ($\mathbf{1}^{HS–LS}$), CCDC -684269 ($\mathbf{2}^{HS}$·MeOH), CCDC -684270 ($\mathbf{2}^{HS–LS}$·MeOH), CCDC -973145 ($\mathbf{3}^{HS}$·1.5Tol), CCDC -973146 ($\mathbf{3}^{HS}$·MeOH), CCDC -973147 ($\mathbf{4}^{HS}$·0.25MeOH), CCDC -973149

Table 5. Single-crystal diffraction data and parameters of compounds $\mathbf{1}^{HS}$, $\mathbf{1}^{HS-LS}$, $\mathbf{2}^{HS}$·MeOH, $\mathbf{2}^{HS-LS}$·MeOH, $\mathbf{3}^{HS}$·1.5Tol.

Compound	$\mathbf{1}^{HS}$	$\mathbf{1}^{HS-LS}$	$\mathbf{2}^{HS}$·MeOH	$\mathbf{2}^{HS-LS}$·MeOH	$\mathbf{3}^{HS}$·1.5Tol
Fe^{II} spin state	HS	HS-LS	HS	HS-LS	HS
Formula	$C_{33}H_{36}FeN_4O_6$	$C_{66}H_{72}Fe_2N_8O_{12}$	$C_{32}H_{36}FeN_4O_5$	$C_{64}H_{72}Fe_2N_8O_{10}$	$C_{85}H_{92}Fe_2N_8O_{12}$
M_r [g mol^{-1}]	640.51	1281.02	612.50	1225.00	1529.37
λ [Å]	0.70930	0.71069	0.71069	0.71069	0.70930
T [K]	200	100	225	125	200
Crystal system	monoclinic	monoclinic	monoclinic	monoclinic	triclinic
Space group	P 21/c	P 21/c	C 2/c	P 21/c	$P\bar{1}$
a [Å]	12.292(6)	19.714(5)	17.861(4)	17.857(5)	12.7120(13)
b [Å]	18.983(8)	18.697(5)	15.197(3)	15.105(5)	13.0428(13)
c [Å]	16.256(5)	16.196(5)	22.713(5)	22.214(6)	13.8537(15)
α [°]	90.00	90.00	90.00	90.00	68.631(10)
β [°]	126.59(2)	95.047(5)	97.918(1)	98.077(2)	75.539(9)
γ [°]	90.00	90.00	90.00	90.00	68.030(10)
V [Å^3]	3046(2)	5947(3)	6106.3(2)	5932.3(3)	1966.5(4)
Z	4	4	8	4	1
$\rho_{calcd.}$ [Mg m^{-3}]	1.397	1.431	1.332	1.372	1.291
μ [mm]$^{-1}$	0.547	0.560	0.540	0.556	0.435
$F(000)$	1344	2688	2576	2576	806
$2\Theta_{max}$ [°]	50.62	50.74	54.96	50.65	49.47
Data/restraints/ parameters	5544/0/401	10855/0/801	6996/0/386	10807/0/768	6707/93/507
Reflections collected	56020	62758	23796	36238	13020
Independent reflections (R_{int})	5544 (0.0629)	10855 (0.0793)	6996 (0.0471)	10807 (0.0779)	6707 (0.0320)
$R(F)$[a] (all data)	0.0345 (0.0720)	0.0389 (0.0992)	0.0443 (0.0791)	0.0564 (0.1058)	0.0557 (0.1038)
$wR(F^2)$[b] (all data)	0.0796 (0.1011)	0.0743 (0.0998)	0.1056 (0.1206)	0.1309 (0.1544)	0.1350 (0.1469)
GOF	1.058	0.999	1.026	1.023	0.894
Largest diff. peak and hole [e Å^{-3}]	0.451, –0.262	0.511, –0.466	0.335, –0.352	0.857, –0.590	0.587, –0.399

[a] $R(F) = \Sigma||F_o| - |F_c||/\Sigma|F_o|$. [b] $wR(F^2) = [\Sigma[w(F_o^2 - F_c^2)^2]/\Sigma w(F_o^2)^2]^{1/2}$, $w = 1/[\sigma^2(F_o^2) + (aP)^2 + bP]$, where $P = [F_o^2 + 2(F_c^2)]/3$.

Table 6. Single-crystal diffraction data and parameters of compounds $\mathbf{3}^{HS-LS}$·1.5Tol, $\mathbf{3}^{HS}$·MeOH, $\mathbf{4}^{HS}$·0.25MeOH, $\mathbf{4}^{LS}$·0.25MeOH, $\mathbf{5}^{LS/LS}$·MeOH.

Compound	$\mathbf{3}^{HS-LS}$·1.5Tol	$\mathbf{3}^{HS}$·MeOH	$\mathbf{4}^{HS}$·0.25MeOH	$\mathbf{4}^{LS}$·0.25MeOH	$\mathbf{5}^{LS/LS}$·MeOH
Fe^{II} spin state	HS-LS	HS	HS	LS	LS/LS
Formula	$C_{163}H_{176}Fe_4N_{16}O_{24}$	$C_{33}H_{38}FeN_4O_7$	$C_{30.27}H_{31.06}FeN_4O_{4.27}$	$C_{30.25}H_{31}FeN_4O_{4.25}$	$C_{31}H_{34}FeN_4O_7$
M_r [g mol^{-1}]	2966.60	658.52	574.95	574.31	630.47
λ [Å]	0.70930	0.71073	0.71069	0.71069	0.70930
T [K]	130	200	293	7	175
Crystal system	triclinic	triclinic	triclinic	triclinic	triclinic
Space group	$P\bar{1}$	$P\bar{1}$	$P\bar{1}$	$P\bar{1}$	$P\bar{1}$
a [Å]	12.7815(6)	11.7025(3)	11.559(2)	11.037(2)	11.0987(15)
b [Å]	16.7360(6)	12.2137(4)	11.818(3)	11.633(6)	14.6555(13)
c [Å]	18.4934(8)	12.4828(2)	11.951(2)	12.196(2)	19.575(4)
α [°]	94.294(3)	72.9593(15)	76.206(19)	72.949(36)	75.432(11)
β [°]	101.732(3)	80.6512(16)	67.861(16)	65.328(16)	75.985(14)
γ [°]	90.514(3)	70.5753(11)	72.519(17)	71.960(23)	74.820(10)
V [Å^3]	3861.2(3)	1604.6(7)	1427.8(5)	1328.4(8)	2920.7(7)
Z	1	2	2	2	4
$\rho_{calcd.}$ [Mg m^{-3}]	1.276	1.363	1.337	1.436	1.434
μ [mm^{-1}]	0.441	0.523	0.571	0.613	0.572
$F(000)$	1562	692	602	602	1320
$2\Theta_{max}$ [°]	49.53	54.89	50.70	50.70	50.65
Data/restraints/ parameters	13157/7/857	7275/0/412	4714/0/368	4063/0/483	10642/0/788
Reflections collected	24323	13747	7335	6316	50123
Independent reflections (R_{int})	13157 (0.0441)	7275 (0.0310)	4714 (0.0185)	4063 (0.0274)	10642 (0.0808)
$R(F)$[a] (all data)	0.0614 (0.1146)	0.0429 (0.0639)	0.0384 (0.0420)	0.0517 (0.0733)	0.0564 (0.1140)
$wR(F^2)$[b] (all data)	0.1667 (0.1874)	0.0970 (0.1053)	0.0967 (0.0996)	0.0883 (0.0941)	0.1220 (0.1521)
GOF	0.754	1.059	1.146	1.177	1.030
Largest diff. peak and hole [e Å^{-3}]	1.785, –0.746	0.295, –0.425	0.3000, –0.303	0.433, –0.519	0.734, –0.642

[a] $R(F) = \Sigma||F_o| - |F_c||/\Sigma|F_o|$. [b] $wR(F^2) = [\Sigma[w(F_o^2 - F_c^2)^2]/\Sigma w(F_o^2)^2]^{1/2}$, $w = 1/[\sigma^2(F_o^2) + (aP)^2 + bP]$, where $P = [F_o^2 + 2(F_c^2)]/3$.

($\mathbf{4}^{HS-LS}$·0.25MeOH) and CCDC -973149 ($\mathbf{5}^{LS/LS}$·MeOH) contain the supplementary crystallographic data for this paper. These data can be obtained free of charge from The Cambridge Crystallographic Data Centre via www.ccdc.cam.ac.uk/data_request/cif.

Synthesis: The syntheses of the iron(II) complexes were carried out under argon by using Schlenk tube techniques. All solvents were purified as described in the literature[27] and distilled under argon. $[FeL1(MeOH)_2]$ and $[FeL2(MeOH)_2]$ were prepared as described in

the literature.[28] 1,3-Bis(4-pyridyl)propane and 1,2-bis(4-pyridyl)-ethane were purchased from Sigma–Aldrich and used as received, 4,4′-bipyridine was purchased from Acros Organics and used as received.

[FeL1(bppa)] (1): [FeL1(MeOH)$_2$] (0.25 g, 0.49 mmol) and 1,3-bis(4-pyridyl)propane (0.98 g, 4.93 mmol) were dissolved in toluene (15 mL) and heated to reflux for 1 h. After cooling down to room temperature, a fine crystalline black precipitate had formed that was filtered off, washed with toluene (2 × 5 mL) and dried in vacuo (yield: 0.21 g, 67%). Crystals suitable for X-ray analysis formed in the mother liquor within a few weeks. IR (KBr): $\tilde{\nu}$ = 1679 (s) (OC=O) cm^{-1}. MS (DEI-(+), 70 eV): *m*/*z* (%) = 442 (71) [FeL1$^+$], 198 (100) [bppa$^+$]. $C_{33}H_{36}FeN_4O_6$ (640.20): calcd. C 61.88, H 5.67, N 8.75; found C 61.58, H 5.65, N 8.71.

[FeL1(bppa)]·0.25MeOH (1·0.25MeOH): [FeL1(MeOH)$_2$] (1.67 g, 3.30 mmol) and 1,3-bis(4-pyridyl)propane (3.27 g, 16.5 mmol) were dissolved in methanol (25 mL) and heated to reflux for 1 h. After cooling down to room temperature, a fine crystalline black precipitate had formed that was filtered off, washed with methanol (2 × 5 mL) and dried in vacuo (yield: 0.96 g, 46%). $C_{33.25}H_{37}FeN_4O_{6.25}$ (648.52): calcd. C 61.58, H 5.75, N 8.64; found C 61.53, H 5.73, N 8.68.

[FeL2(bppa)]·MeOH (2·MeOH): A mixture of [FeL2(MeOH)$_2$] (0.75 g, 1.96 mmol) and 1,3-bis(4-pyridyl)propane (1.94 g, 9.80 mmol) in methanol (10 mL) was heated to reflux for 1 h. After cooling at 5 °C for 24 h, a crystalline black precipitate was obtained that was filtered off, washed with methanol (2 × 5 mL) and dried in vacuo (yield: 0.75 g, 62%). IR (KBr): $\tilde{\nu}$ = 1642 (s) (C=O) cm^{-1}. MS (DEI-(+), 70 eV): *m*/*z* (%) = 382 (64) [FeL2$^+$], 367 (17) [FeL2$^+$ – CH_3], 198 (89) [bppa$^+$], 93 (100) [bppa$^+$ – C_7H_8N]. MS (ESI): *m*/*z* (%) = 778 (2) [FeL2$^+$ + 2 bppa], 580 (4) [FeL2$^+$ + bppa + H], 199 (100) [bppa$^+$+H]. $C_{32}H_{36}FeN_4O_5$ (612.50): calcd. C 62.75, H 5.92, N 9.15; found C 62.54, H 5.78, N 9.14.

[FeL2(bppa)]·EtOH (2·EtOH): A solution of [FeL2(MeOH)$_2$] (0.52 g, 1.36 mmol) and 1,3-bis(4-pyridyl)propane (1.35 g, 6.81 mmol) in ethanol (60 mL) was heated to reflux for 4 h. After cooling to room temperature, **2**·EtOH was obtained in the form of fine black crystals that were filtered off, washed with ethanol (2 × 5 mL) and dried in vacuo (yield: 0.44 g, 52%). IR (KBr): $\tilde{\nu}$ = 1643 (s) (C=O) cm^{-1}. MS (DEI-(+), 70 eV): *m*/*z* (%) = 382 (96) [FeL2$^+$], 367 (27) [FeL2$^+$ – CH_3], 198 (100) [bppa$^+$]. MS (ESI): *m*/*z* (%) = 580 (4) [FeL2$^+$ + bppa], 199 (100) [bppa$^+$ + H]. $C_{33}H_{38}FeN_4O_5$ (626.52): calcd. C 63.26, H 6.11, N 8.94; found C 63.15, H 5.92, N 9.12.

[FeL1(bpea)] (3): A solution of [FeL1(MeOH)$_2$] (0.26 g, 0.51 mmol) and 1,2-bis(4-pyridyl)ethane (0.95 g, 5.13 mmol) in methanol (30 mL) was heated to reflux for 1 h. After cooling down to room temperature, a brown powder was obtained that was filtered off, washed with methanol (2 × 5 mL) and dried in vacuo (yield: 0.22 g, 69%). $C_{32}H_{34}FeN_4O_6$ (626.48): calcd. C 61.35, H 5.47, N 8.94; found C 61.12, H 5.48, N 8.96.

[FeL1(bpea)]·MeOH (3·MeOH): Crystals of [FeL1(bpea)] suitable for X-ray analysis were obtained from a slow diffusion process by using a Schlenk tube, which was, to a certain height, parcelled by a glass wall into two chambers. [FeL1(MeOH)$_2$] (0.55 g, 1.09 mmol) was placed at the base of one chamber, and 1,2-bis(4-pyridyl)ethane (1.00 g, 5.43 mmol) was placed in the other chamber. Solvent methanol was carefully filled just as high to allow a little diffusion between the chambers. After two weeks, **3**·MeOH was obtained in the form of black crystals. $C_{33}H_{38}FeN_4O_7$ (658.21): calcd. C 60.19, H 5.82, N 8.51; found C 60.17, H 5.52, N 8.71.

[FeL1(bpea)]·Tol (3·1.5Tol): A solution of [FeL1(MeOH)$_2$] (0.22 g, 0.43 mmol) and 1,2-bis(4-pyridyl)ethane (0.81 g, 4.34 mmol) in toluene (15 mL) was heated to reflux for 1 h. After cooling down to room temperature, black crystals of **3**·1.5Tol had formed which were filtered off, washed with toluene (2 × 5 mL) and dried in vacuo (yield: 0.20 g, 62%). IR (KBr): $\tilde{\nu}$ = 1688 (s) (OC=O) cm^{-1}. MS (DEI-(+), 70 eV): *m*/*z* (%) = 442 (100) [FeL1$^+$], 184 (41) [bpea$^+$]. $C_{42.5}H_{46}FeN_4O_6$ (764.69): calcd. C 66.75, H 6.06, N 7.33; found C 66.54, H 5.99, N 7.45.

[FeL2(bpea)] (4): [FeL2(MeOH)$_2$] (0.57 g, 1.28 mmol) and 1,2-bis(4-pyridyl)ethane (2.35 g, 12.8 mmol) were dissolved in methanol (45 mL) and heated to reflux for 1 h. After cooling down to room temperature, a dark brown precipitate was obtained that was filtered off, washed with methanol (2 × 5 mL) and dried in vacuo (yield: 0.50 g, 69%). $C_{30}H_{30}FeN_4O_4$ (566.43): calcd. C 63.61, H 5.34, N 9.89; found C 64.09, H 5.60, N 10.18.

[FeL2(bpea)]·0.25MeOH (4·0.25MeOH): [FeL2(MeOH)$_2$] (0.62 g, 1.62 mmol) and 1,2-bis(4-pyridyl)ethane (1.49 g, 8.11 mmol) were dissolved in methanol (57 mL) and heated to reflux for 1 h. After cooling down to room temperature, a crystalline black precipitate was obtained that was filtered off, washed with methanol (2 × 5 mL) and dried in vacuo (yield: 0.49 g, 53%). Crystals of **4**·0.25MeOH suitable for X-ray analysis were obtained from a slow diffusion process, using methanol solutions of the pyridine (pyr) diadduct [FeL2(pyr)$_2$][13a] (0.15 g, 0.28 mmol) and of bpea (0.26 g, 1.41 mmol) at 50 °C. $C_{30.26}H_{31.06}FeN_4O_{4.26}$ (574.92): calcd. C 63.25, H 5.44, N 9.75; found C 62.51, H 5.55, N 9.60.

[FeL1(bipy)] (5): A solution of [FeL1(MeOH)$_2$] (0.49 g, 0.97 mmol) and 4,4′-bipyridine (1.51 g, 9.68 mmol) in methanol (35 mL) was heated to reflux for 1 h. After cooling down to room temperature, a violet precipitate had formed which was filtered off, washed with methanol (2 × 5 mL) and dried in vacuo (yield: 0.37 g, 64%). $C_{29}H_{29}FeN_4O_6$ (598.43): calcd. C 60.21, H 5.05, N 9.36; found C 60.12, H 5.05, N 9.62.

[FeL1(bipy)]·MeOH (5·MeOH): Crystals of **5**·MeOH were obtained from a slow diffusion process by using methanol solutions of [FeL1(MeOH)$_2$] (0.10 g, 0.19 mmol) and of bipy (0.15 g, 0.94 mmol). After one week, violet acicular crystals had formed. $C_{31}H_{34}FeN_4O_7$ (630.47): calcd. C 59.06, H 5.44, N 8.89; found C 59.04, H 5.12, N 9.11.

Supporting Information (see footnote on the first page of this article): Overview of the magnetic properties of the compounds, the intermolecular hydrogen bonds and nonclassical hydrogen bonds, the short intermolecular contacts, and the thermogravimetric analysis of **5**·MeOH are presented.

Acknowledgments

This work has been supported financially by the Deutsche Forschungsgemeinschaft (SPP 1137 and SPP 1178), the Fonds der Chemischen Industrie and the Center for Integrated Protein Science Munich (CIPSM). The main part of the experiments were done at the University of Munich.

[1] a) H. A. Goodwin, *Coord. Chem. Rev.* **1976**, *18*, 293; b) P. Gütlich, *Struct. Bonding (Berlin)* **1981**, *44*, 83; c) E. König, *Prog. Inorg. Chem.* **1987**, *35*, 527; d) P. Gütlich, A. Hauser, *Coord. Chem. Rev.* **1990**, *97*, 1; e) E. König, *Struct. Bonding (Berlin)* **1991**, *76*, 51; f) P. Gütlich, A. Hauser, H. Spiering, *Angew. Chem. Int. Ed. Engl.* **1994**, *33*, 2024, and references cited therein; g) P. Gütlich, J. Jung, H. Goodwin in *Molecular*

Magnetism: From Molecular Assemblies to the Devices (Eds.: E. Coronado, J. S. Miller, D. Gatteschi, P. Delhaès), NATO ASI Series E: Applied Sciences, **1996**, *321*, p. 327; h) P. Gütlich, H. A. Goodwin (Eds.), "Spin Crossover in Transition Metal Compounds I–III" in *Topics in Current Chemistry*, Springer-Verlag Berlin Heidelberg New York **2004**; i) J. A. Real, A. B. Gaspar, M. C. Munoz, *Dalton Trans.* **2005**, 2062; j) O. Sato, J. Tao, Y.-Z. Zhang, *Angew. Chem.* **2007**, *119*, 2200; *Angew. Chem. Int. Ed.* **2007**, *46*, 2152.

[2] a) O. Kahn, C. Jay Martinez, *Science* **1998**, *279*, 44; b) O. Kahn, C. Jay, J. Kröber, R. Claude, F. Grolière, *Patent* **1995** EP0666561; c) J.-F. Létard, O. Nguyen, N. Daro, *Patent* **2005** FR0512476; d) J.-F. Létard, P. Guionneau, L. Goux-Capes, *Topics in Current Chemistry* (Ed.: P. Gütlich et H. A. Goodwin), Springer Vienna New York, **2004**, *235*, p. 221; e) A. Galet, A. B. Gaspar, M. C. Munoz, G. V. Bukin, G. Levchenko, J. A. Real, *Adv. Mater.* **2005**, *17*, 2949.

[3] J. A. Real, A. B. Gaspar, V. Niel, M. C. Munoz, *Coord. Chem. Rev.* **2003**, *236*, 121.

[4] a) B. Weber, *Coord. Chem. Rev.* **2009**, *253*, 2432–2449; b) B. Weber, E.-G. Jäger, *Eur. J. Inorg. Chem.* **2009**, 465.

[5] B. Weber, W. Bauer, J. Obel, *Angew. Chem. Int. Ed.* **2009**, *47*, 10098.

[6] a) J. A. Real, A. B. Gaspar, M. C. Munoz, P. Gütlich, V. Ksenofontov, H. Spiering, *Topics in Current Chemistry* (Ed.: P. Gütlich et H. A. Goodwin), Springer Vienna New York, **2004**, *233*, p. 167; b) A. B. Gaspar, M. C. Munoz, J. A. Real, *J. Mater. Chem.* **2006**, *16*, 2522; c) A. Bousseksou, G. Molnar, J. A. Real, K. Tanaka, *Coord. Chem. Rev.* **2007**, *251*, 1822.

[7] S. Zein, S. A. Borshch, *J. Am. Chem. Soc.* **2005**, *127*, 16197.

[8] a) Y. Garcia, O. Kahn, L. Rabardel, B. Chansou, L. Salmon, J.-P. Tuchagues, *Inorg. Chem.* **1999**, *38*, 4663; b) G. S. Matouzenko, J.-F. Letard, S. Lecocq, A. Bousseksou, L. Capes, L. Salmon, M. Perrin, O. Kahn, A. Collet, *Eur. J. Inorg. Chem.* **2001**, 2935; c) W. Hibbs, P. J. van Koningsbruggen, A. M. Arif, W. W. Shum, J. S. Miller, *Inorg. Chem.* **2003**, *42*, 5645; d) P. Poganiuch, S. Decurtins, P. Gütlich, *J. Am. Chem. Soc.* **1990**, *112*, 3270; e) L. Wiehl, *Acta Crystallogr., Sect. B* **1993**, *49*, 289; f) R. Hinek, H. Spiering, D. Schollmeyer, P. Gütlich, A. Hauser, *Chem. Eur. J.* **1996**, *2*, 1427; g) B. Weber, C. Carbonera, C. Desplanches, J.-F. Létard, *Eur. J. Inorg. Chem.* **2008**, 1589.

[9] a) M. Mikami, M. Konno, Y. Saito, *Chem. Phys. Lett.* **1979**, *63*, 566; b) N. Sasaki, T. Kambara, *Phys. Rev. B* **1989**, *40*, 2442; c) A. Bousseksou, J. Nasser, J. Linares, K. Boukheddaden, F. Varret, *J. Phys. I* **1992**, *2*, 1381; d) H. Spiering, T. Kohlhaas, H. Romstedt, A. Hauser, C. Bruns-Yilmaz, P. Gütlich, *Coord. Chem. Rev.* **1999**, *190–192*, 629.

[10] a) V. Petrouleas, J.-P. Tuchagues, *Chem. Phys. Lett.* **1987**, *137*, 21; b) D. Boinnard, A. Bousseksou, A. Dworkin, J.-M. Savariault, F. Varret, J.-P. Tuchaugues, *Inorg. Chem.* **1994**, *33*, 271; c) K. Boukheddaden, J. Linares, H. Spiering, F. Varret, *Eur. Phys. J. B* **2000**, *15*, 317; d) D. Chernyshov, M. Hostettler, K. W. Törnroos, H. B. Bürgi, *Angew. Chem.* **2003**, *115*, 3955; *Angew. Chem. Int. Ed.* **2003**, *42*, 3825.

[11] J. J. M. Amoore, C. J. Kepert, J. D. Cashion, B. Moubaraki, S. M. Neville, K. S. Murray, *Chem. Eur. J.* **2006**, *12*, 8220.

[12] S. M. Neville, B. A. Leita, G. J. Halder, C. Kepert, B. Moubaraki, J.-F. Letard, K. S. Murray, *Chem. Eur. J.* **2008**, *14*, 10123.

[13] a) B. Weber, E. Kaps, J. Weigand, C. Carbonera, J.-F. Letard, K. Achterhold, F.-G. Parak, *Inorg. Chem.* **2008**, *47*, 487; b) B. Weber, C. Carbonera, C. Desplanches, J.-F. Létard, *Eur. J. Inorg. Chem.* **2008**, 1589; c) B. Weber, E. S. Kaps, C. Desplanches, J.-F. Létard, K. Achterhold, F.-G. Parak, *Eur. J. Inorg. Chem.* **2008**, 4891.

[14] a) B. Weber, R. Tandon, D. Himsl, *Z. Anorg. Allg. Chem.* **2007**, *633*, 1159; b) B. Weber, E. S. Kaps, C. Desplanches, J.-F. Létard, *Eur. J. Inorg. Chem.* **2008**, 2963.

[15] a) B. Weber, E. Kaps, *Heteroat. Chem.* **2005**, *16*, 391; b) B. Weber, F.-A. Walker, *Inorg. Chem.* **2007**, *46*, 6794; c) B. Weber, E. S. Kaps, J. Obel, K. Achterhold, F. G. Parak, *Inorg. Chem.* **2008**, *47*, 10779.

[16] W. Bauer, B. Weber, *Inorg. Chim. Acta* **2009**, *362*, 2341.

[17] P. J. van Koningsbruggen, Y. Garcia, O. Kahn, L. Fournès, H. Kooijman, A. L. Spek, J. G. Haasnoot, J. Moscovici, K. Provost, A. Michalowicz, F. Renz, P. Gütlich, *Inorg. Chem.* **2000**, *39*, 1891.

[18] G. S. Matouzenko, M. Perrin, B. le Guennic, C. Genre, G. Molnar, A. Bousseksou, S. A. Borshch, *Dalton Trans.* **2007**, *9*, 934.

[19] a) G. S. Matouzenko, G. Molnar, N. Brefuel, M. Perrin, A. Bousseksou, S. A. Borshch, *Chem. Mater.* **2003**, *15*, 550; b) C. Genre, G. S. Matouzenko, E. Jeanneau, D. Luneau, *New J. Chem.* **2006**, *30*, 1669.

[20] C. Genre, E. Jeanneau, A. Bousseksou, D. Luneau, S. A. Borshch, G. S. Matouzenko, *Chem. Eur. J.* **2008**, *14*, 697.

[21] J. Linares, H. Spiering, F. Varret, *Eur. Phys. J. B* **1999**, *10*, 271.

[22] a) A. B. Koudriavtsev, A. F. Strassen, J. G. Haasnoot, M. Grunert, P. Weinberger, W. Linert, *Phys. Chem. Chem. Phys.* **2003**, *5*, 3676; b) A. B. Koudriavtsev, A. F. Strassen, J. G. Haasnoot, M. Grunert, P. Weinberger, W. Linert, *Phys. Chem. Chem. Phys.* **2003**, *5*, 3666.

[23] A. Altomare, M. C. Burla, G. M. Camalli, G. Cascarano, C. Giacovazzo, A. Guagliardi, A. G. G. Moliterni, G. Polidori, R. Spagna, *SIR 97*, Campus Universitario Bari, **1997**; A. Altomare, M. C. Burla, G. M. Camalli, G. Cascarano, C. Giacovazzo, A. Guagliardi, A. G. G. Moliterni, G. Polidori, R. Spag, *J. Appl. Crystallogr.* **1999**, *32*, 115.

[24] G. M. Sheldrick, *SHELXL 97*, University of Göttingen, Germany, **1993**.

[25] C. K. Johnson, M. N. Burnett, *ORTEP-III*, Oak-Ridge National Laboratory, Oak-Ridge, TN (USA) **1996**; L. J. Farrugia, *J. Appl. Crystallogr.* **1997**, *30*, 565.

[26] E. Keller, *SCHAKAL-99*, University of Freiburg, Freiburg, Germany, **1999**.

[27] Autorenkollektiv: *Organikum*, Johann Ambrosius Barth Verlagsgesellschaft mbH **1993**.

[28] E.-G. Jäger, E. Häussler, M. Rudolph, M. Rost, *Z. Anorg. Allg. Chem.* **1985**, *525*, 67.

Received: December 29, 2010
Published Online: March 25, 2011

